17. We thank D. S. Campbell for careful reading of the manuscript, C. Krull for the pMES–internal ribosome entry site (IRES)–EGFP vector, J. G. Flanagan for APTag-2 vector, H. Fujisawa for helpful discussions, and the Developmental Studies Hybridoma Bank for antibodies. This work was supported by grants-in-aid from the Ministry of Education, Science, Sports, and Culture of Japan (MEXT), by the 21st Century COE Program and by the Global COE Program (Cell Fate Regulation Research and Education Unit), MEXT, Japan.

Supporting Online Material

www.sciencemag.org/cgi/content/full/323/5912/388/DC1
Materials and Methods
Figs. S1 to S12
Tables S1 and S2
Movie S1

27 August 2008; accepted 2 December 2008
10.1126/science.1165187

Developmental Biology 337 (2010) 405–414

Contents lists available at ScienceDirect

Developmental Biology

journal homepage: www.elsevier.com/developmentalbiology

Cv2, functioning as a pro-BMP factor via twisted gastrulation, is required for early development of nephron precursors

Makoto Ikeya [a,*,1], Kumi Fukushima [a], Masako Kawada [a], Sachiko Onishi [b], Yasuhide Furuta [c], Shigenobu Yonemura [b], Toshio Kitamura [d], Tetsuya Nosaka [e], Yoshiki Sasai [a,*]

[a] Organogenesis and Neurogenesis Group, RIKEN Center for Developmental Biology, 2-2-3 Minatojima-minamimachi, Chuo, Kobe 650-0047, Japan
[b] Electron Microscope Laboratory, RIKEN Center for Developmental Biology, Kobe 650-0047, Japan
[c] Department of Biochemistry and Molecular Biology, M.D. Anderson Cancer Center, University of Texas, Houston, TX 77030, USA
[d] Division of Cellular Therapy, The Institute of Medical Science, University of Tokyo, Tokyo 108-8639, Japan
[e] Department of Microbiology, Mie University Graduate School of Medicine, Tsu, Mie 514-8507, Japan

ARTICLE INFO

Article history:
Received for publication 8 July 2009
Revised 8 November 2009
Accepted 9 November 2009
Available online 13 November 2009

Keywords:
BMP
Kidney
Organogenesis
Genetic interactions

ABSTRACT

The fine-tuning of BMP signals is critical for many aspects of complex organogenesis. In this report, we show that the augmentation of BMP signaling by a BMP-binding secreted factor, Crossveinless2 (Cv2), is essential for the early embryonic development of mammalian nephrons. In the *Cv2*-null mouse, the number of cap condensates (clusters of nephron progenitors, which normally express Cv2) was decreased, and the condensate cells exhibited a reduced level of aggregation. In these $Cv2^{-/-}$ condensates, the level of phosphorylated Smad1 (pSmad1) was substantially lowered. The loss of a *Bmp7* allele in the $Cv2^{-/-}$ mouse enhanced the cap condensate defects and further decreased the level of pSmad1 in this tissue. These observations indicated that Cv2 has a pro-BMP function in early nephrogenesis. Interestingly, the renal defects of the $Cv2^{-/-}$ mutant were totally suppressed by a null mutation of *Twisted gastrulation* (*Tsg*), which encodes another BMP-binding factor, showing that Cv2 exerts its pro-BMP nephrogenic function Tsg-dependently. By using an embryonic kidney cell line, we presented experimental evidence showing that Cv2 enhances pro-BMP activity of Tsg. These findings revealed the molecular hierarchy between extracellular modifiers that orchestrate local BMP signal peaks in the organogenetic microenvironment.

Introduction

In terrestrial amniotes, the kidney is an indispensable and complex organ that maintains fluid homeostasis and blood pressure. Its anlage is a tissue called the metanephros. In the mouse, metanephric development starts about embryonic day (E) 10.5 with the demarcation of the metanephric blastema in the caudal part of the intermediate mesoderm, followed by reciprocal inductions between the blastema and the Wolffian duct (**Vainio and Lin, 2002**). In response to metanephric blastema-derived signals, the ureteric bud forms from the Wolffian duct, invades the metanephric blastema, and successively branches to form the collecting ducts. Conversely, ureteric bud-derived signals induce the formation of metanephric blastema-derived condensates (cap condensates) around the tips of collecting ducts; the cells forming the condensates will ultimately give rise to the nephrons, which carry out the functions of the adult kidney (**Kobayashi et al., 2008**). Although the signaling networks that regulate duct branching have been extensively studied (**Shah et al., 2004**), relatively little is known about the molecular mechanism of how cap condensates are formed and maintained (**Kobayashi et al., 2008; Oxburgh et al., 2004**).

The Bone Morphogenetic Protein (BMP) family is a class of secreted signaling proteins that belong to the transforming growth factor-beta (TGFβ) superfamily; they have diverse effects on the control of embryogenesis, including kidney development (**Cain et al., 2008; Godin et al., 1998; Hogan, 1996; Simic and Vukicevic, 2005**). An intriguing feature of BMP signaling is the presence of various extracellular BMP inhibitors (i.e., anti-BMP factors), such as Chordin, Noggin, Follistatin, Cerberus, and Gremlin (**Glinka et al., 1997; Hemmati-Brivanlou et al., 1994; Hsu et al., 1998; Lamb et al., 1993; Sasai et al., 1995, 1994; Smith and Harland, 1992**). Moreover, recent studies show that there are some proteins that bind to BMPs extracellularly and augment their signaling (i.e., pro-BMP factors). One protein with pro-BMP functions is Crossveinless2 (Cv2; also called Bmper), which enhances BMP signaling during wing cross-vein formation in *Drosophila*, as well as in neural crest emigration in the chick embryo, dorsal-ventral patterning of the zebrafish gastrula, and some cultured cell lines (**Coles et al., 2004; Conley et al., 2000; Kamimura et al., 2004; Kelley et al., 2009; Moser et al., 2007; Rentzsch et al., 2006; Serpe et al., 2008**).

* Corresponding authors. Fax: +81 78 306 1854.
E-mail addresses: mikeya@cdb.riken.jp (M. Ikeya), yoshikisasai@cdb.riken.jp (Y. Sasai).
[1] Present address: Department of Cell Modulation, Institute of Molecular Embryology and Genetics, Kumamoto University, Honjo 2-2-1, Kumamoto 860-0811, Japan.

0012-1606/$ – see front matter © 2009 Elsevier Inc. All rights reserved.
doi:10.1016/j.ydbio.2009.11.013

Interestingly, other reports have shown Cv2 to have an anti-BMP role in various in vitro and in vivo contexts (**Ambrosio et al., 2008**; **Binnerts et al., 2004**; **Coles et al., 2004**; **Harada et al., 2008**; **Kelley et al., 2009**; **Moser et al., 2003**; **Rentzsch et al., 2006**; **Zhang et al., 2007, 2008**). For instance, Cv2 exerts both pro- and anti-BMP activities when injected into the zebrafish embryo (**Rentzsch et al., 2006**). In the *Xenopus* gastrula, Cv2 acts predominantly as an anti-BMP factor (**Ambrosio et al., 2008**). While endocytic internalization is proposed to contribute to Cv2's anti-BMP activity, this machinery appears to be restricted to a limited range of cell types (**Kelley et al., 2009**). Biochemical and crystal structure analyses suggest that vertebrate Cv2 may interfere with BMP ligand-receptor binding via its Chordin-type cysteine-rich domain (CR1; **Zhang et al., 2007**; **Zhang et al., 2008**), although the in vivo relevance of such molecular interactions remains elusive. More recently, Cv2 was shown to bind other proteins, such as Chordin (**Ambrosio et al., 2008**), suggesting that Cv2's function is complex, and its role as a pro- or anti-BMP factor may be context-dependent. Therefore, careful investigation is required to identify the in vivo role of Cv2 in different developmental contexts.

Previously, by showing a genetic enhancement between *Bmp4* and *Cv2*, we demonstrated that Cv2 functions as a pro-BMP factor in vertebral and eye development (**Ikeya et al., 2006**). In the same study, we found kidney defects (hypoplasia) in *Cv2*-null mouse embryos. Our previous report showed that Cv2 acts in the same direction with Kcp, which functions as a pro-BMP factor in a different context (**Ikeya et al., 2006**; **Lin et al., 2005**). However, our previous study could not tell whether Cv2 in the developing kidney was required as a pro- or anti-Bmp factor, because of the lack of genetic evidences showing functional interaction between Cv2 and Bmp ligands.

Here, we report that Cv2 plays an essential role as a pro-BMP factor in mouse kidney development. We found that Cv2 promotes the BMP-dependent formation of the cap condensates, and we present genetic evidence that the pro-BMP function of Cv2 is dependent on the presence of Tsg, another BMP modulator. These results demonstrate that an extracellular system for modulating local BMP signals via Cv2 and Tsg plays a key role in the early steps of mouse nephron development.

Materials and methods

Mutant mice and crosses

Mice carrying mutations in *Cv2*, *Bmp7*, *Tsg*, and *Smad1* were described previously (**Hayashi et al., 2002**; **Ikeya et al., 2006**; **Luo et al., 1995**; **Nosaka et al., 2003**). We crossed $Cv2^{+/-}$ mice with $Bmp7^{+/-}$, $Tsg^{-/-}$ or $Smad1^{+/-}$ mice to obtain compound heterozygotes. No obvious defects were observed in the compound heterozygotes, and we used them for further intercrosses. Genotypes were confirmed by PCR (**Ikeya et al., 2006, 2008**). Animals were housed in environmentally controlled rooms in accordance with RIKEN guidelines for animal experiments.

LacZ staining, histology, immunohistochemistry, and statistics

LacZ staining, histology, and immunohistochemistry were performed as described previously (**Ikeya et al., 2006**). Primary antibodies and dilutions were as follows: anti-alpha-catenin, 1:500 (Sigma, rabbit polyclonal); anti-BF2, 1:500 (Abcam, goat polyclonal); anti-cadherin-11, 1:500 (R&D, goat polyclonal); anti-Cv2, 1:1000 (R&D, goat polyclonal); anti-E-cadherin, 1:500 (Takara, ECCD2); anti-β-galactosidase, 1:5000 (Cappel, rabbit polyclonal) or 1:2000 (AbD Serotec, goat polyclonal); anti-laminin, 1:500 (Chemicon, AL-4); anti-NCAM, 1:1000 (Chemicon, rabbit polyclonal); anti-Pax2, 1:200 (Zymed, rabbit polyclonal); anti-phospho-Smad1/5/8, 1:30 (Cell Signaling, rabbit polyclonal); and anti-WT1, 1:50 (Santa Cruz, rabbit polyclonal). For staining with the anti-WT1 antibody, citrate buffer, pH 6, was used for antigen retrieval (Zymed) in a 2100 Retriever (PickCell Laboratories). The anti-Cv2 polyclonal antibody recognizes both N- and C-halves of cleaved Cv2 (data not shown).

The signal intensity of the phospho-Smad1/5/8 staining was compared as follows, using the ImageJ software (National Institutes of Health, Bethesda, MD). We stained sections with phospho-Smad1/5/8-specific antibody and DAPI and acquired images by scanning the sections with a confocal microscope (LSM510 (Zeiss)). The images were trimmed into smaller ones showing either cap condensates or collecting ducts, and we divided the total signal intensity of phospho-Smad1/5/8 in the trimmed regions by DAPI-positive area. We defined this value as the "average signal intensity" of phospho-Smad1/5/8 and compared it across images. No differences were observed among the average signal intensities of the collecting ducts, regardless of the genotype. We regarded average signal intensities from cap condensates that were less than two thirds of the collecting duct average intensity as "reduced."

The numbers of nephrons and nephron progenitors at E18.5 were counted as described previously (**Ikeya et al., 2006**). We scored eight to 20 embryos of each genotype to obtain these numbers. The number of LacZ-positive cap condensates at E13.5, 14.5, and 15.5 was obtained from six to 30 kidneys from each genotype.

Statistical analyses were performed using GraphPad Prism 4 (GraphPad Software).

Cell culture, transfection, siRNA, and luciferase assay

HEK293T cells were maintained in DMEM/10% FCS (HyClone). To examine the effect of Cv2 on BMP signaling, reverse transfections were performed in a 24-well cell culture plate (BD Falcon) using FuGene6 (Roche, Basel, Switzerland) with a total of 210 ng DNA [100 ng of BRE-luc (**Korchynskyi and ten Dijke, 2002**), 10 ng of phRL-null (Promega), and the indicated dose of CIG-mCv2 and CIG-LacZ (**Megason and McMahon, 2002**)] per well, in DMEM/1% FCS. Annealed and purified siRNA duplexes were obtained from Ambion (Austin, TX) and were added at 75 ng per well 4 h prior to the cDNA transfection with X-treme Gene (Roche, Basel, Switzerland). After 16 h of treatment, the cells were lysed and assayed for luciferase activity using the dual luciferase reporter assay system (Promega, Madison, WI), according to the manufacturer's instructions.

Results

Enhancement of hypoplastic phenotypes in the $Cv2^{-/-}$ kidney by $Bmp7^{+/-}$ mutation

We previously demonstrated that *Cv2*-null mice display a reduced kidney size and lower nephron number than wild-type mice (**Ikeya et al., 2006**). To examine the role of Cv2 during nephrogenesis, we first analyzed *Cv2*'s expression patterns during kidney development in *nLacZ*-knock-in mice ($Cv2^{+/nLacZ}$). At E11.5, the metanephric blastema expressed $Cv2^{nLacZ}$, whereas the ureteric buds were negative for it (**Figs. 1A–C**). At E12.0, the maturating stromal cells located in the central portion of the kidney became $Cv2^{nLacZ}$-negative (asterisk in **Fig. 1D**). At E13.5 and E14.5, the $Cv2^{nLacZ}$ expression was mainly restricted to the cap condensates (**Figs. 1E–H**, and data not shown) and to portions of the forming nephrons (pretubular aggregates, comma-shaped body, and S-shaped body) and Bowman's capsules (**Supplementary Figs. S1A–D**). Immunohistochemical analyses confirmed that cap condensate cells positive for Pax2 strongly expressed $Cv2^{nLacZ}$, but the peripheral stroma, which was positive for BF2, and collecting ducts did not (**Supplementary Figs. S2A–C**). From E14 until birth, the $Cv2^{nLacZ}$ expression was restricted to the cap condensates and its derivatives (data not shown).

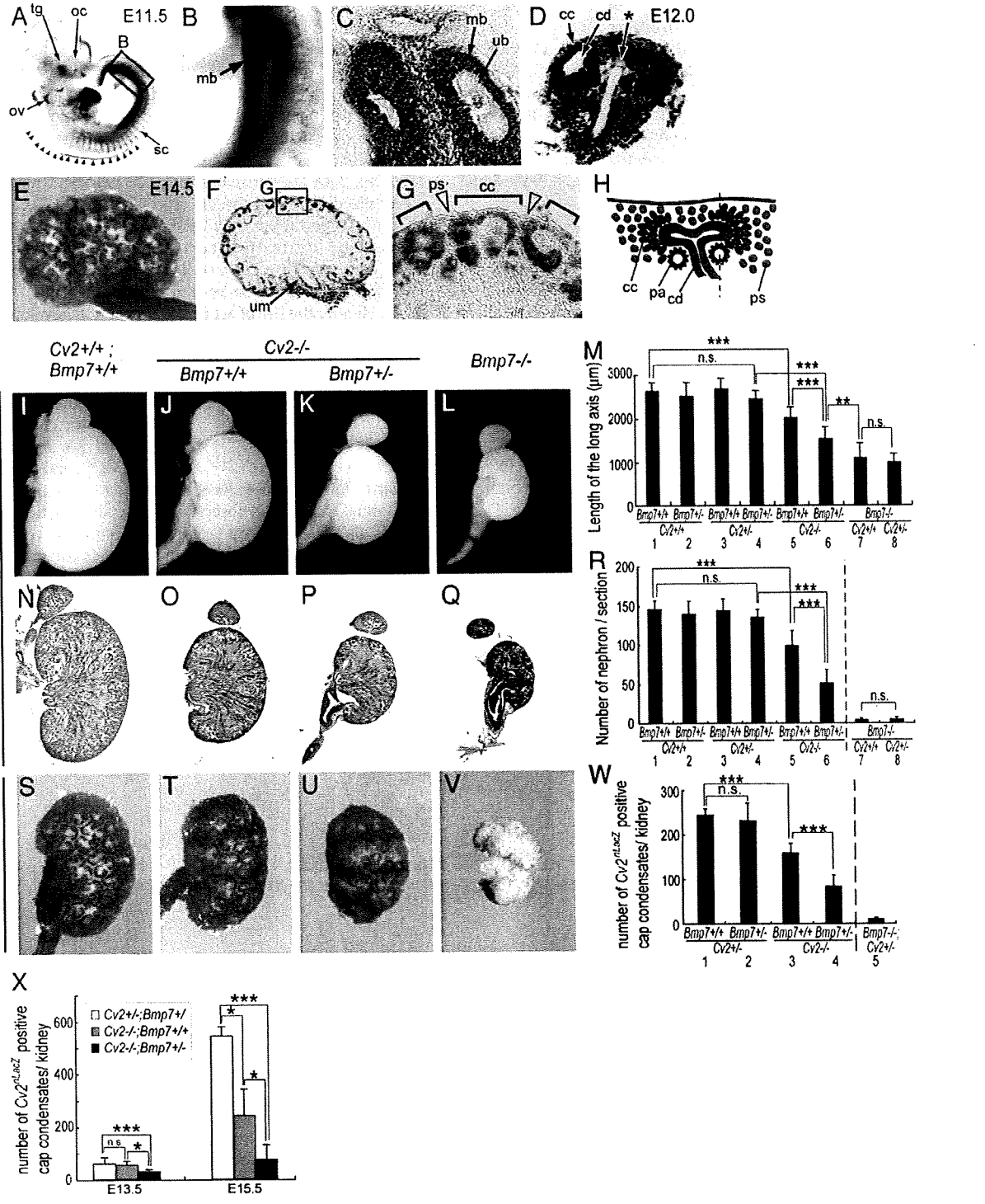

Fig. 1. Cooperative roles of *Cv2* and *Bmp7* in kidney development. (A–G) Expression of *Cv2* analyzed with *nLacZ* knock-in mice. (A–C) At E11.5, LacZ staining was observed in the trigeminal ganglion (tg), optic cup (oc), otic vesicle (ov), sclerotome (sc), roof plate of the neural tube (triangles), and metanephric blastema (mb), but not in the ureteric bud (ub). (D) At E12.0, the central portion of the metanephric mesenchyme became $Cv2^{nLacZ}$ negative (asterisk). cd, collecting duct; cc, cap condensates. (E–G) At E14.5, $Cv2^{nLacZ}$ was preferentially expressed in the cap condensates (bracket in G) and the ureteric mesenchyme (um). Triangles in (G) indicate that the peripheral stroma (ps) was $Cv2^{nLacZ}$-negative. (H) Schematic representation of the cortical region of the embryonic kidney. pa, pretubular aggregate. (I–L) External appearances of the control, $Cv2^{-/-}$, $Bmp7^{+/-}$;$Cv2^{-/-}$, and $Bmp7^{-/-}$ kidneys at E18.5. (M) Length of the long axis. (N–Q) Longitudinal sections stained with hematoxylin and eosin at E18.5. (R) The number of nephrons in the maximal longitudinal sections. (S–V) External views at E14.5 stained with $Cv2^{nLacZ}$. (W, X) The number of $Cv2^{nLacZ}$-positive cap condensates at E14.5 (W, Tukey test), and E13.5 and E15.5 (X, Bonferroni test). Error bars show S.D.; n.s., no significant difference; $^{***}P<0.001$; $^{**}P<0.01$; $^{*}P<0.05$. In (R) and (W), statistical analyses of the $Bmp7^{-/-}$ samples were performed separately because of significant differences among the S.D.s.

Although these expression patterns, as well as the *Cv2*-null phenotypes, suggest a crucial role for Cv2 in nephrogenesis, the molecular mechanism of Cv2's action, and particularly whether it functioned as a pro-BMP or anti-BMP factor in this developmental context, was unclear. Among the *Bmp* genes, *Bmp7* is strongly expressed in the cap condensate, as well as in the ureteric bud, collecting duct, and forming nephron (**Supplementary Fig. S3A**; **Dudley and Robertson, 1997**; **Godin et al., 1998**), and its mutation causes progressive renal hypoplasia (**Dudley et al., 1995**; **Luo et al., 1995**). In addition, Cv2 binds BMP7 with a high affinity (**Zhang et al., 2007**). These findings suggested that Cv2 might interact with BMP7 in kidney development. We therefore tested their functional interaction by crossing *Cv2* mutants with *Bmp7* mutants (**Figs. 1I–X**).

At E18.5, the loss of one allele of *Bmp7* in the $Cv2^{+/+}$ or $Cv2^{+/-}$ background had no obvious effects on kidney development (**Figs. 1M, R, lanes 1–4**). Similarly, the loss of one *Cv2* allele in the $Bmp7^{-/-}$ background had little effect on kidney size or nephron number (**Figs. 1M, R, lanes 7, 8**). In contrast, the deletion of a single *Bmp7* allele in the $Cv2^{-/-}$ background caused further reductions in the kidney size and nephron number at E18.5 than seen in $Cv2^{-/-}$ mice at the same age (**Figs. 1J, K, O, P**; **Figs. 1M, R, lanes 5, 6**).

A similar genetically enhanced reduction in the number of cap condensates (marked by the expression of $Cv2^{nLacZ}$) was evident during the early stages of kidney development, even at E14.5 and E15.5 (**Figs. 1S–X**). In addition, the enhanced decrease in the components of the forming nephrons (comma- and S-shaped bodies) was obvious in the $Bmp7^{+/-};Cv2^{-/-}$ kidney, particularly at E15.5 (**Fig. 1X** and **Supplementary Fig. S4**).

These observations support the idea that Cv2 plays a pro-BMP role in the early phases of nephron formation.

Cv2 is essential for high levels of BMP signaling in cap condensates

These findings prompted us to study the expression and functions of Cv2 proteins in the early embryonic kidney. To this end, we performed immunohistochemical analysis of Cv2 protein in the developing kidney (**Fig. 2**). At E12.5 and E14.5, the Cv2 protein had accumulated in two regions: the pericellular region of the $Cv2^{nLacZ}$-expressing cap condensates (punctate signals; arrows in Figs. 2G–I) and the basement membrane of the collecting ducts (continuous signals; arrowheads in **Figs. 2B, E**). No immunostaining was observed in the $Cv2^{-/-}$ kidney, demonstrating the specificity of the antibody (**Fig. 2F**). Both the pericellular and the basement membrane signals co-localized with fibronectin (**Figs. 2G–I**) and laminin (data not shown), suggesting that Cv2 protein is densely accumulated in the extracellular matrix. This finding is in accordance with the previous work demonstrating Cv2's co-localization with extracellular matrix (**Rentzsch et al., 2006**; **Serpe et al., 2008**).

To identify the site of action of Cv2 in renal development, we next analyzed the levels of intracellular BMP signaling in wild-type and mutant mice by detecting a downstream component of BMP signaling, phosphorylated Smad1/5/8 (pSmad1), which is frequently used to assay BMP activity. At E14.5, high pSmad1 signals were observed in both the cap condensates (cc) and the tips of the collecting ducts (cd) in wild-type and $Bmp7^{+/-}$ embryos (**Fig. 3A** and **Supplementary Fig. S5**). In contrast, in $Cv2^{-/-}$, $Bmp7^{+/-};Cv2^{-/-}$, and $Bmp7^{-/-}$ embryos, pSmad1 staining was reduced in the cap condensates, whereas no substantial change was observed in the collecting ducts (Figs. 3B–D). **Fig. 3I** shows the percentages of cap condensates with reduced pSmad1 signals (in this analysis, signal levels comparable to those in the collecting duct cells were considered to be high). As shown

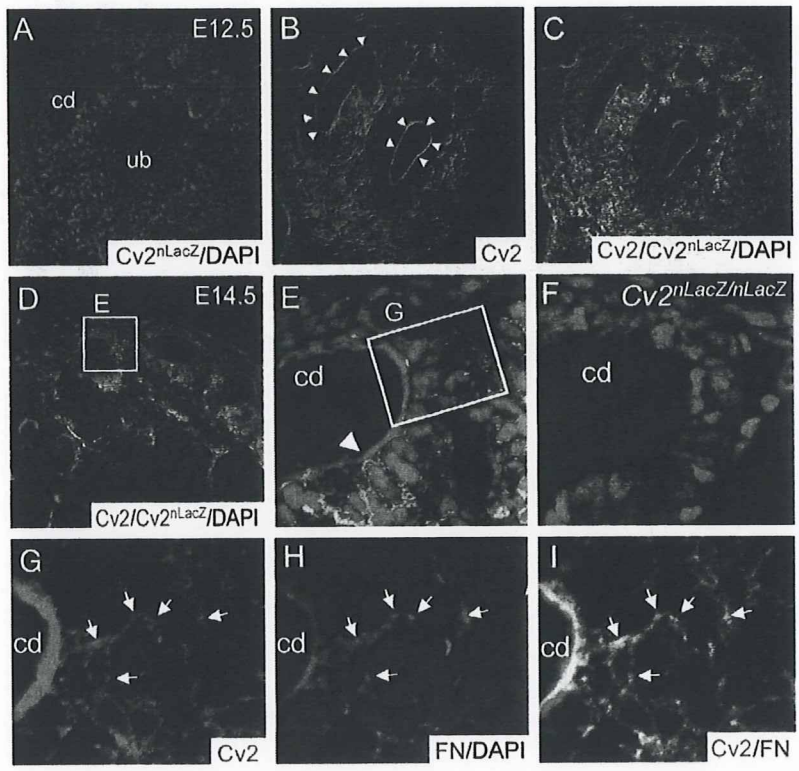

Fig. 2. Distribution of the Cv2 protein. Cv2 protein was accumulated in both the pericellular region of the cap condensate and the basement membrane of the collecting duct. (A–C) Immunohistochemistry with anti-Cv2 antibody at E12.5. Arrowheads, accumulation of Cv2 on the surface of the collecting duct and ureteric bud. (D–I) At E14.5, anti-Cv2 staining was observed in the pericellular region of the $Cv2^{nLacZ}$-positive cells (arrows in G–I) and the basement membrane of the collecting duct (arrowhead in E). (F) No signal was detected in the $Cv2^{-/-}$ mutants. Punctate pericellular signals co-localized with fibronectin (FN; arrows in G–I).

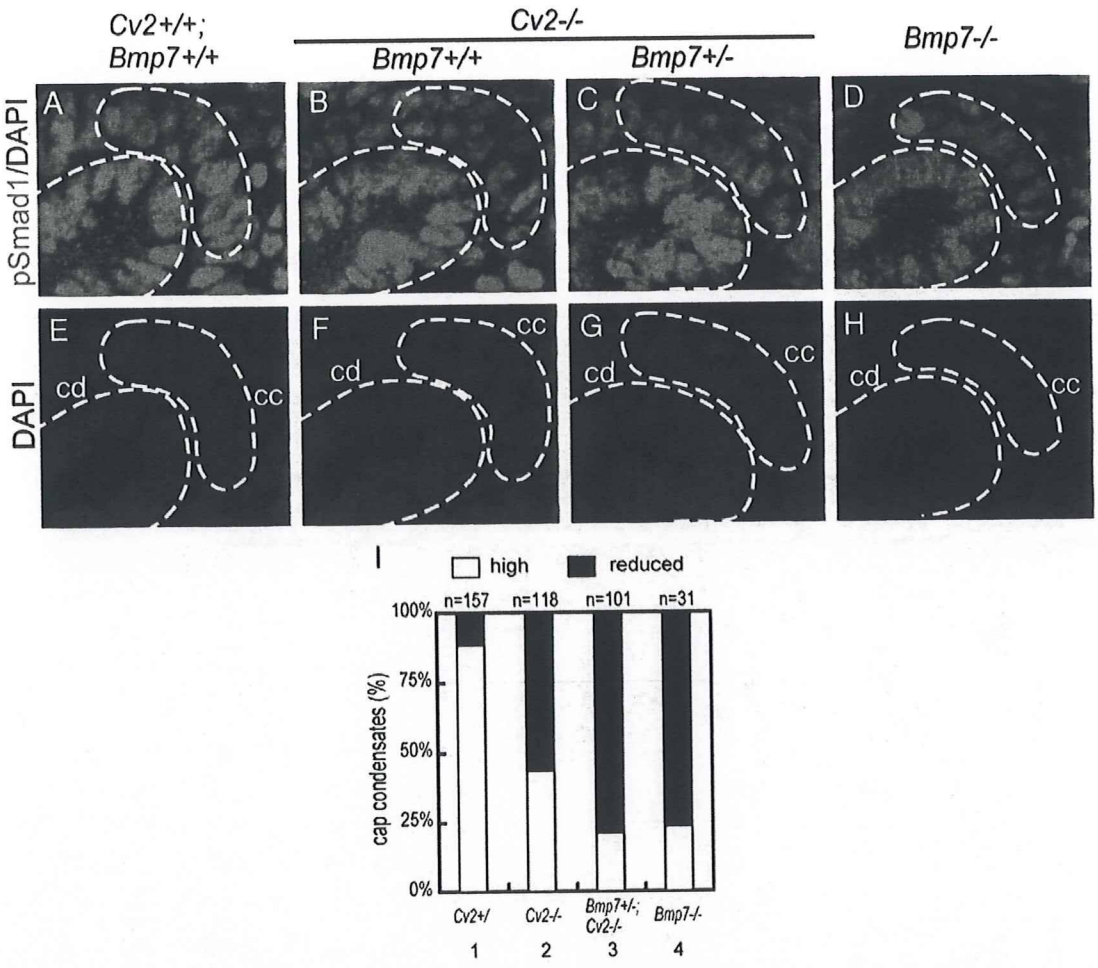

Fig. 3. A pro-BMP role of *Cv2* in the cap condensates but not in the collecting ducts. Staining intensity of pSmad1 was decreased in cap condensates of $Cv2^{-/-}$, $Bmp7^{+/-};Cv2^{-/-}$, and $Bmp7^{-/-}$ kidneys, but it was unchanged in the collecting ducts from all genotypes. Blue, DAPI; red, phospho-Smad1/5/8 (pSmad1)-specific antibody. (I) Percentages of cap condensates showing reduced pSmad1 signal intensity. Under the $Cv2^{-/-}$ background, the $Bmp7^{+/+}$ and $Bmp7^{+/-}$ groups exhibited a significant differences (P value = 0.0007) by Chi-square test.

(Fig. 3I, lanes 2 and 3), the additional deletion of one *Bmp7* allele enhanced the reduction of pSmad1 in the $Cv2^{-/-}$ background, suggesting that Cv2 acts in the same direction as BMP7 (i.e., as a pro-BMP factor).

These observations indicate that Cv2 is essential for enhancing BMP signals in the cap condensate during kidney organogenesis, but that the high BMP signals in the collecting ducts are independent of Cv2, suggesting a tissue-specific mode of Cv2's action.

Incomplete cellular aggregation in the $Cv2^{-/-}$ cap condensates

During nephrogenesis, cap condensates are formed as compact cell aggregates at the tips of the collecting ducts (cc in **Fig. 4**A). As shown above, BMP signaling was attenuated in the cap condensates of $Cv2^{-/-}$ and $Bmp7^{+/-};Cv2^{-/-}$ mutants. In addition, thin section analysis revealed impaired cell–cell attachment in the $Cv2^{-/-}$ and $Bmp7^{+/-};Cv2^{-/-}$ cap condensates (see loosely packed aggregates in **Figs. 4**B, C; E14.5), although the cells looked healthy and did not exhibit signs of apoptosis such as picnosis. These observations indicate that the loss of Cv2's pro-BMP function not only reduced the cap condensate number but also caused abnormal cellular aggregation.

Next, we further examined the cellular aggregation by immunostaining. While adhesion molecules such as NCAM and cadherin11 (also alpha-catenin) were distributed uniformly in the cell–cell interface regions in the cap condensate of control embryos (**Figs. 4**E, I, M), these protein appeared discontinuous or punctate in the $Cv2^{-/-}$ and $Bmp7^{+/-};Cv2^{-/-}$ mutants (arrowheads in **Figs. 4**F, G, J, K, N, O). These changes did not seem to be caused by a loss of specific cell types, since the cell type-specific markers (Pax2 and p75 for the cap condensate and BF2 for the peripheral stroma) were expressed normally in these mice (**Figs. 4**Q–S, and data not shown). Rather, these results indicate that a local augmentation of BMP signaling by Cv2 is crucial for the proper formation of cap condensates, including the cap–cell aggregation, during kidney development.

To focus in on which developmental step was most dependent on Cv2, we investigated the marker expression and aggregation of the cap cells in the $Bmp7^{-/-}$ kidney. We found, as reported previously, that the number of $Pax2^{+}$ cells in the $Bmp7^{-/-}$ cap condensates was severely reduced (**Fig. 4**T; **Dudley et al., 1995; Luo et al., 1995**). The adhesion molecules were found in a discontinuous pattern (**Figs. 4**H, L, P), resembling those in the *Cv2* mutants. In addition, the morphology of $Bmp7^{-/-}$ cap condensates were substantially impaired (even more drastically than $Cv2^{-/-}$ and $Bmp7^{+/-};Cv2^{-/-}$ condensates), consisting of cells with a generally round shape (**Fig. 4**D). These results imply that the complete loss of BMP7 signaling affected the cap condensate in terms of both the cellular presence (Pax2 expression; as reported previously (**Dudley et al., 1995; Dudley and Robertson, 1997; Luo et al., 1995**)) and the formation of the aggregates. In contrast, the

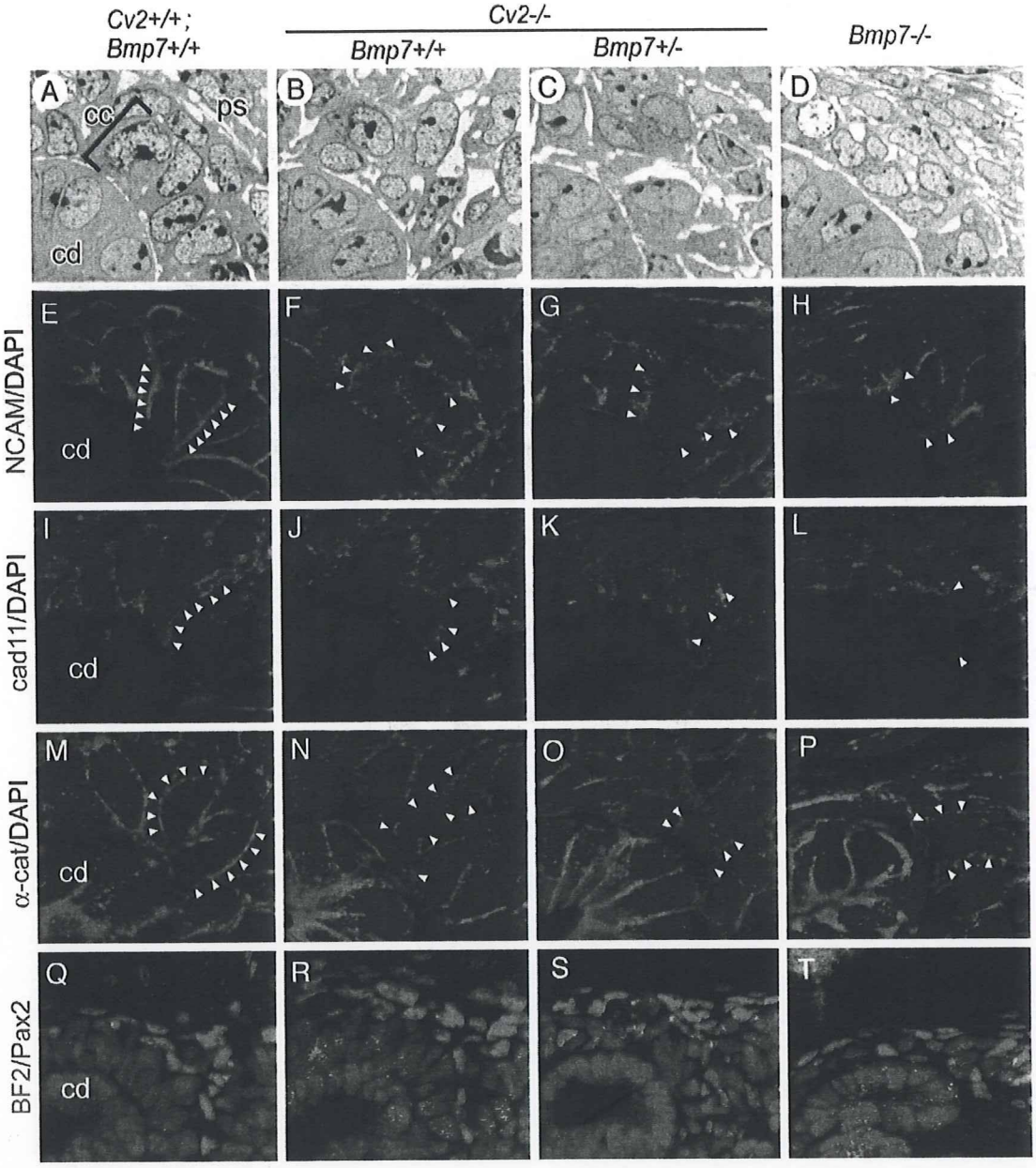

Fig. 4. Cv2 required for the cellular aggregation of the cap condensates. (A–D) Plastic thin sections stained with toluidine blue. In $Cv2^{-/-}$ and $Bmp7^{+/-};Cv2^{-/-}$ kidneys, cap condensate cells adhered loosely to one another. In the $Bmp7^{-/-}$ kidney, the cells on the tip of the collecting duct became round. (E–P) Disturbed distribution of adhesion proteins in the cap condensates of the mutants. Immunohistochemistry with (E–H) anti-NCAM, (I–L) anti-cadherin11, and (M–P) anti-alpha-catenin. (Q–T) Immunohistochemistry with anti-Pax2 (green) and anti-BF2 (red). The Pax2-positive cap condensates and collecting ducts and the BF2-positive peripheral stroma developed normally in the $Cv2^{-/-}$ and $Bmp7^{+/-};Cv2^{-/-}$ mutants. In the $Bmp7^{-/-}$ kidney, the number of Pax2-positive cells was markedly reduced.

attenuation of BMP signaling caused by the loss of Cv2 preferentially impaired the formation of the cellular aggregates.

Tsg mutation is epistatic to the Cv2 mutation in the kidney-defect phenotype

Taken together, our genetic and histochemical analyses demonstrated that Cv2 is an essential pro-BMP factor for the development of cap condensates in the early embryonic kidney. An obvious remaining question is how Cv2 promotes BMP signaling in these cells.

Very recently, two independent studies (from De Robertis' and our groups) reported a genetic interaction between *Cv2* and *Tsg* in skeletal development (Ikeya et al., 2008; Zakin et al., 2008). The major skeletal defects of the *Cv2*-null mutant mice (in the thoracic and lumbar vertebrae) are suppressed in $Tsg^{-/-};Cv2^{-/-}$ embryos, which show moderate skeletal phenotypes (Nosaka et al., 2003; Petryk et al., 2004; Zakin and De Robertis, 2004). This suggests that the *Tsg* mutation is epistatic to the *Cv2* mutation in skeletal development. However, the precise molecular and cellular mechanism of this gene interaction in embryonic development was still unknown.

With this in mind, we examined possible interactions between *Cv2* and *Tsg* in kidney development (*Tsg* expression is detected diffusely in the developing kidney (Supplementary Fig. S3B; Nosaka et al., 2003)). In nephrogenesis, as opposed to skeletal development, interactions with the *Tsg* mutation can be analyzed rather simply, because the *Tsg* mutation itself does not cause significant embryonic kidney

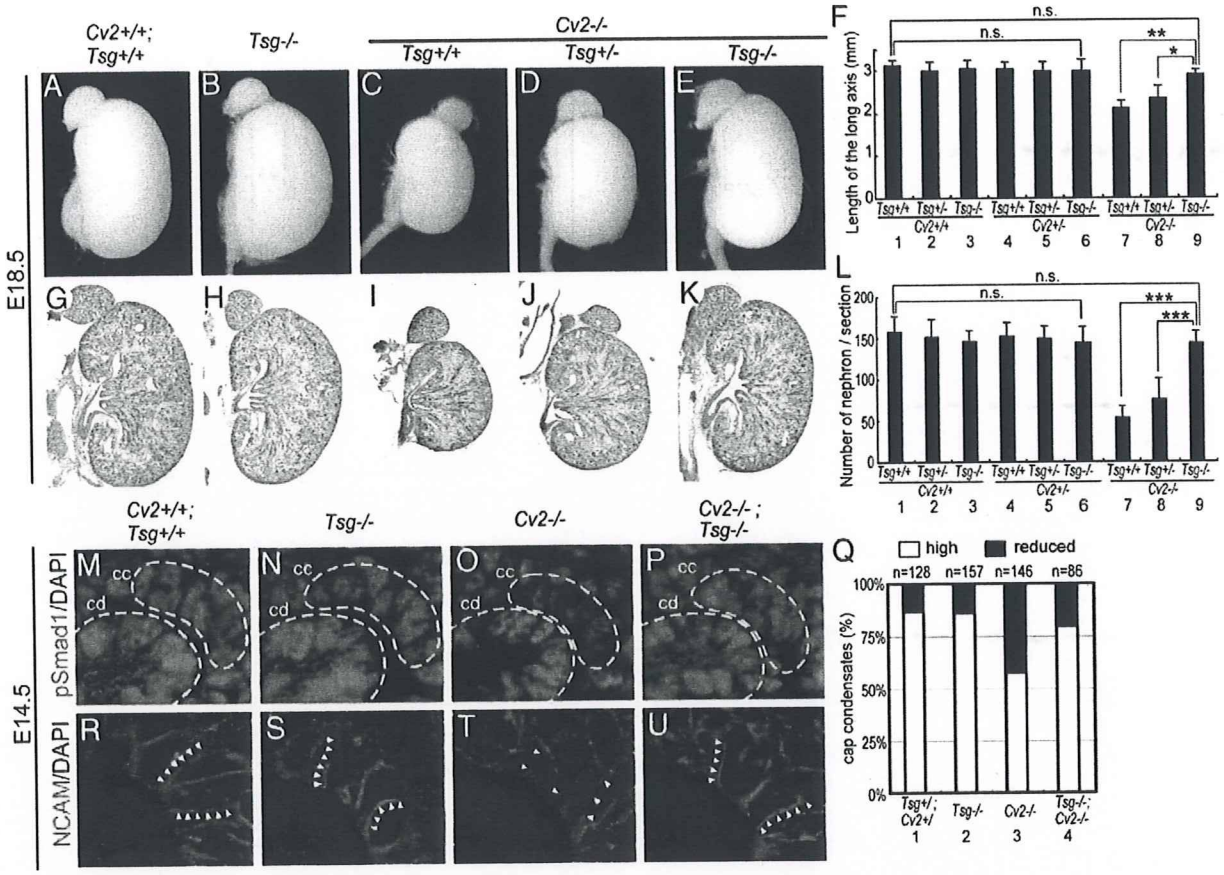

Fig. 5. Evidence for a *Tsg*-dependent pro-BMP function of *Cv2* in vivo. Renal phenotypes of $Cv2^{-/-}$ rescued by the deletion of both alleles of *Tsg* at E18.5 and E14.5. (A–E) External views at E18.5. (F) Length of the long axis. (G–K) Histological sections at E18.5. (L) The number of nephrons in the maximal longitudinal sections. (M–P) Immunohistochemistry with anti-pSmad1 at E14.5. (Q) Percentages of cap condensates exhibiting reduced pSmad1 signal intensity. (R–U) Immunohistochemistry with anti-NCAM at E14.5. Error bars show S.D.; n.s., no significant difference; $***P<0.001$; $**P<0.01$; $*P<0.05$ (Bonferroni test).

phenotypes (Nosaka et al., 2003). In the $Cv2^{+/+}$ and $Cv2^{+/-}$ backgrounds, the loss of both *Tsg* alleles did not significantly affect kidney size or nephron number at E18.5 (Figs. 5A, B, G, H; Figs. 5F, L, lanes 1–6). In contrast, when combined with the $Cv2^{-/-}$ mutation, the elimination of *Tsg* completely suppressed the renal defects otherwise present in *Cv2*-null mutants (Figs. 5C–E, I–K; Figs. 5F, L, lanes 1, 7–9). The *Tsg* deletion also restored the levels of BMP signaling (reduced pSmad1 levels) in the cap condensates of *Cv2*-null mutants at E14.5 (Figs. 5M–Q) and rescued the impaired cell–cell adhesion in the condensates (Figs. 5R–U).

These in vivo findings suggest a unidirectional dependence in which the pro-BMP function of Tsg requires Cv2, while Cv2 function is not dependent on Tsg activity.

Tsg-dependent mechanism of Cv2's pro-BMP function in cultured embryonic kidney cells

The suppression of the $Cv2^{-/-}$ kidney phenotypes by the *Tsg* mutation implied that, as a whole, Cv2 and Tsg act in opposite directions. That is, they appeared to play pro-BMP and anti-BMP roles, respectively, during nephrogenesis. Interestingly, previous studies suggested that Tsg can act as an anti-BMP or pro-BMP factor, depending on the context (Chang et al., 2001; Harland, 2001; Larrain et al., 2001; Oelgeschlager et al., 2000; Ross et al., 2001; Scott et al., 2001). For instance, genetic interaction studies of mouse *Tsg*-null mutations with *Bmp4* and *Bmp7* mutations show *Tsg* acting as a pro-BMP factor in head development and posterior mesodermal patterning (Zakin and De Robertis, 2004; Zakin et al., 2005). In *Xenopus* embryos, the Chordin–Tsg complex binds to BMPs and inhibits their signaling more efficiently than Chordin, an anti-BMP factor, does alone (anti-BMP activity of Tsg; Oelgeschlager et al., 2000; Scott et al., 2001). In the presence of the Chordin-degrading enzyme Xolloid, on the other hand, Tsg dislodges BMP from cleaved Chordin fragments, resulting in enhanced BMP signaling (a pro-BMP activity; Oelgeschlager et al., 2000).

Given the context-dependent bidirectional functions of Tsg and our findings in this study, the following hypothetical models could explain the functional interaction between Cv2 and Tsg in nephrogenesis. (1) The pro-BMP factor Cv2 and the anti-BMP factor Tsg act independently on BMP signals as simple antagonists (Fig. 6A, Model a). (2) Cv2 acts as a pro-BMP factor by interfering with the anti-BMP function of Tsg (Fig. 6A, Model b). (3) Tsg has simultaneous dual functions as both a pro-BMP and an anti-BMP factor, while Cv2 acts as a co-factor to strengthen the pro-BMP aspect of Tsg's functions (Fig. 6A, Model c).

Given that the fine-tuning of BMP signals is vital for kidney organogenesis (Cain et al., 2008), the phenotypical discrepancy between the normal kidney development of $Tsg^{-/-}$ embryos and the marked hypoplasia of *Cv2*-null embryos is rather difficult to explain with hypothetical Models a and b, which predict hyperactive BMP levels in $Tsg^{-/-}$ kidneys. In contrast, the BMP activity level under the $Tsg^{-/-}$ condition would be less affected in the hypothetical Model c, in which the simultaneous loss of both the anti- and pro-BMP functions could reduce the extent of change in signaling strength (Supplementary Fig. S6B). Consistent with this idea, we have not seen substantial changes in pSmad1 levels in $Tsg^{-/-}$ embryonic kidneys compared with control kidneys (Fig. 5N and our preliminary

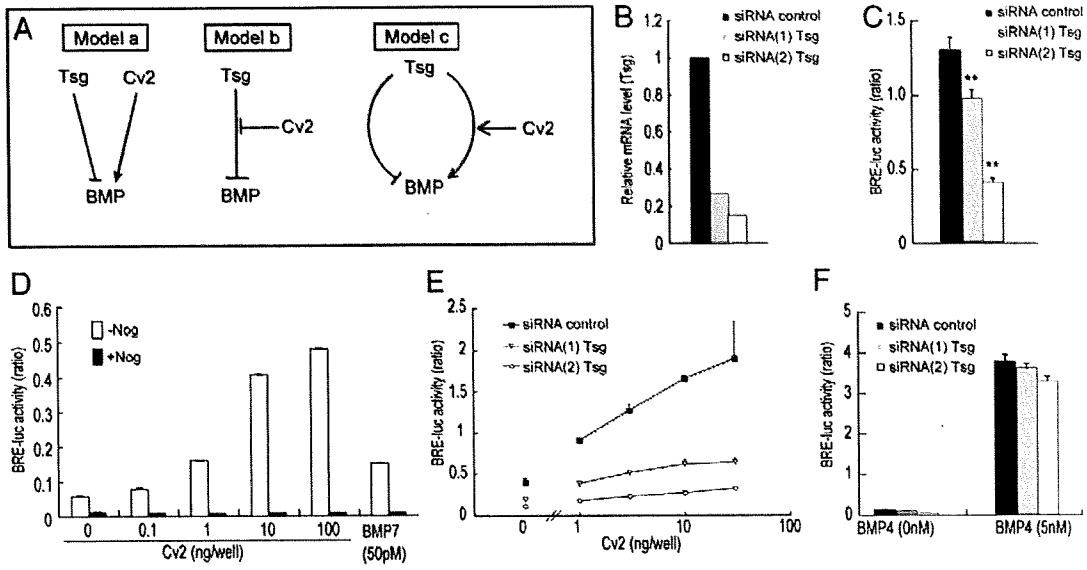

Fig. 6. Cv2 enhances pro-BMP activity of Tsg in HEK293T cell. (A) Models of the interaction between Tsg and Cv2. (B) Knockdown efficiency of Tsg mRNA. Expression levels were determined by quantitative real-time PCR analysis. (C) siRNA targeting of *Tsg* attenuates BMP signaling. Error bars show S.D.; $^{**}P<0.01$ (Dunnet test). (D) Dose-dependent activation of BMP signaling by *Cv2* in HEK293T cells. (E) siRNA targeting of *Tsg* reduces dose-dependent activation of BMP signaling by *Cv2*. (F) *Tsg* knockdown cells respond normally to treatment with high levels BMP4.

observations). Thus, Model c is consistent with the in vivo phenotype, at least in this respect.

To test the predictive ability of this model, one essential question is whether Cv2 can in fact function as a co-factor for the pro-BMP activity of Tsg in kidney development. This question is particularly relevant in light of a *Xenopus* study that suggests that Cv2 enhances the anti-BMP activity of Tsg in a different developmental context (dorsal-ventral patterning during gastrulation) (**Ambrosio et al., 2008**). Therefore, we next examined whether Cv2 promotes BMP signaling under the condition in which Tsg predominantly exerts a pro-BMP activity over an anti-BMP function.

In a series of preliminary experiments, we found that a human embryonic kidney-derived cell line, HEK293T, expresses *Tsg* as well as *Cv2* and *BMPs* (**Supplementary Fig. S7**), and that endogenous Tsg acted predominantly as a pro-BMP factor, since, when Tsg was knocked down by siRNAs (see **Fig. 6B** for the knockdown efficiency), the BMP signaling reporter (*BRE-luc*) activity was reduced accordingly (**Fig. 6C**). In this cell line, the expression of exogenous *Cv2* (introduced by plasmid transfection) strongly augmented the BMP signal in a dose-dependent manner, showing a pro-BMP activity (**Fig. 6D**, open columns). This augmentation appeared to depend on extracellular BMP signaling, since the addition of Noggin to the culture medium completely suppressed it (**Fig. 6D**, closed columns). Importantly, there was little augmentation of BMP signaling by *Cv2* in the *Tsg*-depleted HEK293T cells (**Fig. 6E**). This absence of the *Cv2*-induced increase in the *Tsg*-depleted cells was not owing to a general loss of the cellular BMP signaling pathway, because the *BRE-luc* activity was strongly stimulated by high concentrations of BMP4 also in these cells (**Fig. 6F**).

These data show that Cv2 functions as a pro-BMP factor in the presence of Tsg, which has a pro-BMP role in this embryonic kidney cell line, supporting the idea that Cv2 can enhance the pro-BMP activity of Tsg at least under certain situations (**Fig. 6A**, Model c).

Discussion

In this report, we demonstrated that Cv2 plays an essential pro-BMP role in early nephrogenesis. The cap condensate is the embryonic kidney tissue that normally expresses Cv2, and its development was substantially affected by the *Cv2*-null mutation, even during very early histogenesis. The loss of Cv2 directly attenuated the BMP signaling in this tissue, as assessed by its reduced pSmad1 levels (**Fig. 3**; in contrast, pSmad2 levels were largely unaffected; **Supplementary Fig. S8**). In contrast, the *Cv2* mutation did not substantially affect the high BMP signaling levels in the neighboring collecting duct cells, which do not normally express Cv2. Taken together, these observations suggest that Cv2 is a local (or short-range) enhancer of BMP signaling that mainly acts in a tissue-autonomous fashion. In other words, the tissue augments its own BMP response by expressing Cv2.

At least three mechanistic explanations for the context-dependent pro-BMP function of Cv2 have been advocated so far: (1) a cleaved Cv2 protein, rather than a full-length one, exerts a pro-BMP activity (shown in a zebrafish study; **Rentzsch et al., 2006**). (2) Cv2 is a biphasic BMP modulator acting in a dose-dependent manner that, only at a low dose, facilitates the binding of BMPs to their type I receptor (shown in a *Drosophila* study; **Serpe et al., 2008**). (3) Cv2 increases the local concentration of diffusible Chordin/Tsg/BMP protein complexes (e.g., on the ventral side in the case of the *Xenopus* embryo), which release active BMPs to their cell surface receptors upon the cleavage of Chordin by tolloid proteinases (proposed in a *Xenopus* study; **Ambrosio et al., 2008**). In this case, the entrapment of BMP into the complexes is an anti-BMP process, while the release of BMP from the accumulated Chordin/Tsg/BMP complexes (i.e., reservoir complexes for BMP) serves as a pro-BMP step.

Of the three proposals (which are not mutually exclusive), the last one (Mechanism 3) fits our in vivo and in vitro data particularly well. First, our immunostaining results showed that Cv2 proteins are associated with the pericellular matrix (**Fig. 2**), which could make Cv2 less diffusible. Since Cv2 can physically interact with Chordin, Tsg and BMP (**Ambrosio et al., 2008**), the Cv2-bound pericellular matrix supposedly contributes to the local accumulation of Chordin/Tsg/BMP complexes. Second, the *Cv2*-null mutation specifically affected the cap condensates, which are normally surrounded by auto/paracrine Cv2. Third, Cv2 functions as a pro-BMP factor in the presence of Tsg, which is evidence that Cv2 might function in a complex, as proposed for Mechanism 3.

In addition, Mechanism 3 appears to be compatible with Model c (Fig. 6A), in which pro- and anti-BMP functions of Tsg can co-exist. In this interpretation, which combines Model c and Mechanism 3, Cv2 preferentially enhances the pro-BMP activity of Tsg; this activity is expected to depend heavily on the Cv2-mediated local high concentration of reservoir complexes that potentially release BMP. In contrast, the inactivation of BMPs by their entrapment in the Chordin–Tsg complex (anti-BMP) is Cv2-independent presumably because the entrapment process itself does not require the specific localization of the complexes. By using an embryonic kidney cell line, in which the pro-BMP function of Tsg is predominantly observed (Fig. 6E), we presented the practical feasibility of Model c (Fig. 6A), at least with respect to the cooperative pro-BMP function of Cv2 and Tsg. Consistent with Model c and also Mechanism 3, Cv2 exerts pro-BMP function in the presence of Tsg in this cell culture system. In the future investigations, other models must also be ruled out, including one in which Cv2 acts as an inhibitor of Tsg's anti-BMP activity, rather than as a co-factor of its pro-BMP activity (a sort of fusion of Models b and c).

This report mainly focused on the pro-BMP role of Cv2. Genetic analyses of *Bmp7;Cv2* mutants provide firm evidences that Cv2 acts predominantly as a pro-BMP factor in early nephrogenesis. In addition, a genetic enhancement in the nephron number was observed between *Cv2* and *Smad1* (Supplementary Fig. S9), indicating that Cv2 works cooperatively not only with the extracellular BMP ligand (BMP7) but also with the major transducer of BMP receptor signaling. Although these data do not argue the presence of a minor anti-BMP function of Cv2, it is considered the total Cv2 activity, at least on balance, is deviated toward the pro-BMP direction in the context of kidney development.

This report also focused on its genetic interactions with Tsg. Whereas it is beyond the scope of this genetics-based study, identifying the detailed molecular mechanisms underlying the pro-BMP function at the protein level is an important topic for future comprehensive study (Umulis et al., 2009). For instance, it will be intriguing to show the different kinetics of BMP release from complexes of Cv2 with Tsg versus Cv2 with Chordin, or the concentration or presentation of the ligand-bearing complexes to the receptor. It is also interesting to learn whether the role of mammalian Tsg in kidney development in fact depends on Chordin, especially given that Chordin and Chordin-related genes are expressed in the embryonic kidney (Supplementary Fig. S10). Because good antibodies for immunohistochemical studies of Tsg, Chordin and the tolloids are not available (our preliminary observations), we cannot currently examine whether Tsg–Chordin complexes are concentrated or specifically degraded near the cap condensate. Visualizing the dynamic localization, diffusion and processing of the complex proteins is a challenging but critical future task.

Our preliminary study showed that the decrease of nephron numbers in $Cv2^{-/-}$ kidneys (E14.5) was also moderately enhanced by adding a $Bmp4^{+/-}$ mutation similar to that observed with $Bmp7^{+/-}$ mutation (Supplementary Fig. S11). On the other hand, during late nephrogenesis, the $Bmp4^{+/-}$ mutation strongly enhanced the hydroureter phenotypes in the $Cv2^{-/-}$ kidneys (Supplementary Fig. S12). In this case, the formation of the ureter mesenchyme, which expresses *Bmp4* but not *Bmp7*, was strongly inhibited, suggesting that BMP4 cooperates with Cv2 independently of BMP7, at least in this context. Thus, whether BMP7 acts as a homodimer or a heterodimer with BMP4 in the Cv2 interaction is a remaining question for further investigation.

Conclusion

From our in vivo and in vitro observations, we conclude that Cv2, in concert with Tsg, shapes the signaling landscape in the complex organogenetic microenvironment of the kidney, creating locally restricted peaks in the BMP signal.

Acknowledgments

We are grateful to the staff of the Laboratory of Animal Resources and Genetic Engineering at the Center for Developmental Biology for their help with mouse husbandry, and to Drs. H. Enomoto, M. Eiraku, H. Inomata, and A. Takai for invaluable comments and discussion. BRE-luc and CIG were kindly provided by Drs. P. ten Djike and A. McMahon, respectively. *Smad1* knockout mice were a kind gift of Dr. K Hayashi through Dr. M. Saitou. MI is thankful to Ayumi Ikeya and Yu-ichi Ikeya for constant encouragement and support during this study. This work was supported in part by grants-in-aid from the Ministry of Education, Culture, Sports, Science and Technology of Japan (Y.S. and M.I.), the Kobe Cluster Project, and the Leading Project (Y.S.), and by the Special Postdoctoral Researchers Program of RIKEN (M.I.).

Appendix A. Supplementary data

Supplementary data associated with this article can be found, in the online version, at doi:10.1016/j.ydbio.2009.11.013.

References

Ambrosio, A.L., Taelman, V.F., Lee, H.X., Metzinger, C.A., Coffinier, C., De Robertis, E.M., 2008. Crossveinless-2 Is a BMP feedback inhibitor that binds Chordin/BMP to regulate Xenopus embryonic patterning. Dev. Cell 15, 248–260.

Binnerts, M.E., Wen, X., Cante-Barrett, K., Bright, J., Chen, H.T., Asundi, V., Sattari, P., Tang, T., Boyle, B., Funk, W., Rupp, F., 2004. Human Crossveinless-2 is a novel inhibitor of bone morphogenetic proteins. Biochem. Biophys. Res. Commun. 315, 272–280.

Cain, J.E., Hartwig, S., Bertram, J.F., Rosenblum, N.D., 2008. Bone morphogenetic protein signaling in the developing kidney: present and future. Differentiation 76, 831–842.

Chang, C., Holtzman, D.A., Chau, S., Chickering, T., Woolf, E.A., Holmgren, L.M., Bodorova, J., Gearing, D.P., Holmes, W.E., Brivanlou, A.H., 2001. Twisted gastrulation can function as a BMP antagonist. Nature 410, 483–487.

Coles, E., Christiansen, J., Economou, A., Bronner-Fraser, M., Wilkinson, D.G., 2004. A vertebrate crossveinless 2 homologue modulates BMP activity and neural crest cell migration. Development 131, 5309–5317.

Conley, C.A., Silburn, R., Singer, M.A., Ralston, A., Rohwer-Nutter, D., Olson, D.J., Gelbart, W., Blair, S.S., 2000. Crossveinless 2 contains cysteine-rich domains and is required for high levels of BMP-like activity during the formation of the cross veins in Drosophila. Development 127, 3947–3959.

Dudley, A.T., Robertson, E.J., 1997. Overlapping expression domains of bone morphogenetic protein family members potentially account for limited tissue defects in BMP7 deficient embryos. Dev. Dyn. 208, 349–362.

Dudley, A.T., Lyons, K.M., Robertson, E.J., 1995. A requirement for bone morphogenetic protein-7 during development of the mammalian kidney and eye. Genes Dev. 9, 2795–2807.

Glinka, A., Wu, W., Onichtchouk, D., Blumenstock, C., Niehrs, C., 1997. Head induction by simultaneous repression of Bmp and Wnt signalling in Xenopus. Nature 389, 517–519.

Godin, R.E., Takaesu, N.T., Robertson, E.J., Dudley, A.T., 1998. Regulation of BMP7 expression during kidney development. Development 125, 3473–3482.

Harada, K., Ogai, A., Takahashi, T., Kitakaze, M., Matsubara, H., Oh, H., 2008. Crossveinless-2 controls bone morphogenetic protein signaling during early cardiomyocyte differentiation in P19 cells. J. Biol. Chem. 283, 26705–26713.

Harland, R.M., 2001. Developmental biology. A twist on embryonic signalling. Nature 410, 423–424.

Hayashi, K., Kobayashi, T., Umino, T., Goitsuka, R., Matsui, Y., Kitamura, D., 2002. SMAD1 signaling is critical for initial commitment of germ cell lineage from mouse epiblast. Mech. Dev. 118, 99–109.

Hemmati-Brivanlou, A., Kelly, O.G., Melton, D.A., 1994. Follistatin, an antagonist of activin, is expressed in the Spemann organizer and displays direct neuralizing activity. Cell 77, 283–295.

Hogan, B.L., 1996. Bone morphogenetic proteins: multifunctional regulators of vertebrate development. Genes Dev. 10, 1580–1594.

Hsu, D.R., Economides, A.N., Wang, X., Eimon, P.M., Harland, R.M., 1998. The Xenopus dorsalizing factor Gremlin identifies a novel family of secreted proteins that antagonize BMP activities. Mol. Cell 1, 673–683.

Ikeya, M., Kawada, M., Kiyonari, H., Sasai, N., Nakao, K., Furuta, Y., Sasai, Y., 2006. Essential pro-Bmp roles of crossveinless 2 in mouse organogenesis. Development 133, 4463–4473.

Ikeya, M., Nosaka, T., Fukushima, K., Kawada, M., Furuta, Y., Kitamura, T., Sasai, Y., 2008. Twisted gastrulation mutation suppresses skeletal defect phenotypes in Crossveinless 2 mutant mice. Mech. Dev. 125, 832–842.

Kamimura, M., Matsumoto, K., Koshiba-Takeuchi, K., Ogura, T., 2004. Vertebrate crossveinless 2 is secreted and acts as an extracellular modulator of the BMP signaling cascade. Dev. Dyn. 230, 434–445.
Kelley, R., Ren, R., Pi, X., Wu, Y., Moreno, I., Willis, M., Moser, M., Ross, M., Podkowa, M., Attisano, L., Patterson, C., 2009. A concentration-dependent endocytic trap and sink mechanism converts Bmper from an activator to an inhibitor of Bmp signaling. J. Cell Biol. 184, 597–609.
Kobayashi, A., Valerius, M.T., Mugford, J.W., Carroll, T.J., Self, M., Oliver, G., McMahon, A.P., 2008. Six2 defines and regulates a multipotent self-renewing nephron progenitor population throughout mammalian kidney development. Cell Stem Cell 3, 169–181.
Korchynskyi, O., ten Dijke, P., 2002. Identification and functional characterization of distinct critically important bone morphogenetic protein-specific response elements in the Id1 promoter. J. Biol. Chem. 277, 4883–4891.
Lamb, T.M., Knecht, A.K., Smith, W.C., Stachel, S.E., Economides, A.N., Stahl, N., Yancopolous, G.D., Harland, R.M., 1993. Neural induction by the secreted polypeptide noggin. Science 262, 713–718.
Larrain, J., Oelgeschlager, M., Ketpura, N.I., Reversade, B., Zakin, L., De Robertis, E.M., 2001. Proteolytic cleavage of Chordin as a switch for the dual activities of twisted gastrulation in BMP signaling. Development 128, 4439–4447.
Lin, J., Patel, S.R., Cheng, X., Cho, E.A., Levitan, I., Ullenbruch, M., Phan, S.H., Park, J.M., Dressler, G.R., 2005. Kielin/chordin-like protein, a novel enhancer of BMP signaling, attenuates renal fibrotic disease. Nat. Med. 11, 387–393.
Luo, G., Hofmann, C., Bronckers, A.L., Sohocki, M., Bradley, A., Karsenty, G., 1995. BMP-7 is an inducer of nephrogenesis, and is also required for eye development and skeletal patterning. Genes Dev. 9, 2808–2820.
Megason, S.G., McMahon, A.P., 2002. A mitogen gradient of dorsal midline Wnts organizes growth in the CNS. Development 129, 2087–2098.
Moser, M., Binder, O., Wu, Y., Aitsebaomo, J., Ren, R., Bode, C., Bautch, V.L., Conlon, F.L., Patterson, C., 2003. BMPER, a novel endothelial cell precursor-derived protein, antagonizes bone morphogenetic protein signaling and endothelial cell differentiation. Mol. Cell. Biol. 23, 5664–5679.
Moser, M., Yu, Q., Bode, C., Xiong, J.W., Patterson, C., 2007. BMPER is a conserved regulator of hematopoietic and vascular development in zebrafish. J. Mol. Cell. Cardiol. 43, 243–253.
Nosaka, T., Morita, S., Kitamura, H., Nakajima, H., Shibata, F., Morikawa, Y., Kataoka, Y., Ebihara, Y., Kawashima, T., Itoh, T., Ozaki, K., Senba, E., Tsuji, K., Makishima, F., Yoshida, N., Kitamura, T., 2003. Mammalian twisted gastrulation is essential for skeleto-lymphogenesis. Mol. Cell. Biol. 23, 2969–2980.
Oelgeschlager, M., Larrain, J., Geissert, D., De Robertis, E.M., 2000. The evolutionarily conserved BMP-binding protein twisted gastrulation promotes BMP signalling. Nature 405, 757–763.
Oxburgh, L., Chu, G.C., Michael, S.K., Robertson, E.J., 2004. TGFbeta superfamily signals are required for morphogenesis of the kidney mesenchyme progenitor population. Development 131, 4593–4605.
Petryk, A., Anderson, R.M., Jarcho, M.P., Leaf, I., Carlson, C.S., Klingensmith, J., Shawlot, W., O'Connor, M.B., 2004. The mammalian twisted gastrulation gene functions in foregut and craniofacial development. Dev. Biol. 267, 374–386.
Rentzsch, F., Zhang, J., Kramer, C., Sebald, W., Hammerschmidt, M., 2006. Crossveinless 2 is an essential positive feedback regulator of Bmp signaling during zebrafish gastrulation. Development 133, 801–811.
Ross, J.J., Shimmi, O., Vilmos, P., Petryk, A., Kim, H., Gaudenz, K., Hermanson, S., Ekker, S.C., O'Connor, M.B., Marsh, J.L., 2001. Twisted gastrulation is a conserved extracellular BMP antagonist. Nature 410, 479–483.
Sasai, Y., Lu, B., Steinbeisser, H., Geissert, D., Gont, L.K., De Robertis, E.M., 1994. Xenopus chordin: a novel dorsalizing factor activated by organizer-specific homeobox genes. Cell 79, 779–790.
Sasai, Y., Lu, B., Steinbeisser, H., De Robertis, E.M., 1995. Regulation of neural induction by the Chd and Bmp-4 antagonistic patterning signals in Xenopus. Nature 376, 333–336.
Scott, I.C., Blitz, I.L., Pappano, W.N., Maas, S.A., Cho, K.W., Greenspan, D.S., 2001. Homologues of twisted gastrulation are extracellular cofactors in antagonism of BMP signalling. Nature 410, 475–478.
Serpe, M., Umulis, D., Ralston, A., Chen, J., Olson, D.J., Avanesov, A., Othmer, H., O'Connor, M.B., Blair, S.S., 2008. The BMP-binding protein Crossveinless 2 is a short-range, concentration-dependent, biphasic modulator of BMP signaling in Drosophila. Dev. Cell 14, 940–953.
Shah, M.M., Sampogna, R.V., Sakurai, H., Bush, K.T., Nigam, S.K., 2004. Branching morphogenesis and kidney disease. Development 131, 1449–1462.
Simic, P., Vukicevic, S., 2005. Bone morphogenetic proteins in development and homeostasis of kidney. Cytokine Growth Factor Rev. 16, 299–308.
Smith, W.C., Harland, R.M., 1992. Expression cloning of noggin, a new dorsalizing factor localized to the Spemann organizer in Xenopus embryos. Cell 70, 829–840.
Umulis, D., O'Connor, M.B., Blair, S.S., 2009. The extracellular regulation of bone morphogenetic protein signaling. Development 136, 3715–3728.
Vainio, S., Lin, Y., 2002. Coordinating early kidney development: lessons from gene targeting. Nat. Rev. Genet. 3, 533–543.
Zakin, L., De Robertis, E.M., 2004. Inactivation of mouse twisted gastrulation reveals its role in promoting Bmp4 activity during forebrain development. Development 131, 413–424.
Zakin, L., Reversade, B., Kuroda, H., Lyons, K.M., De Robertis, E.M., 2005. Sirenomelia in Bmp7 and Tsg compound mutant mice: requirement for Bmp signaling in the development of ventral posterior mesoderm. Development 132, 2489–2499.
Zakin, L., Metzinger, C.A., Chang, E.Y., Coffinier, C., De Robertis, E.M., 2008. Development of the vertebral morphogenetic field in the mouse: interactions between Crossveinless-2 and twisted gastrulation. Dev. Biol. 323, 6–18.
Zhang, J.L., Huang, Y., Qiu, L.Y., Nickel, J., Sebald, W., 2007. von Willebrand factor type C domain-containing proteins regulate bone morphogenetic protein signaling through different recognition mechanisms. J. Biol. Chem. 282, 20002–20014.
Zhang, J.L., Qiu, L.Y., Kotzsch, A., Weidauer, S., Patterson, L., Hammerschmidt, M., Sebald, W., Mueller, T.D., 2008. Crystal structure analysis reveals how the Chordin family member crossveinless 2 blocks BMP-2 receptor binding. Dev. Cell 14, 739–750.

Biochemical and Biophysical Research Communications 390 (2009) 1001–1006

Contents lists available at ScienceDirect

Biochemical and Biophysical Research Communications

journal homepage: www.elsevier.com/locate/ybbrc

FLT3-ITD induces ara-C resistance in myeloid leukemic cells through the repression of the ENT1 expression

Guilan Jin [a], Hiromichi Matsushita [a,*], Satomi Asai [a], Hideo Tsukamoto [b], Ryoichi Ono [c], Tetsuya Nosaka [c], Takashi Yahata [d], Shinichiro Takahashi [e], Hayato Miyachi [a]

[a] Department of Laboratory Medicine, Tokai University School of Medicine, 143 Shimokasuya, Isehara, Kanagawa 259-1193, Japan
[b] Teaching and Research Support Center, Tokai University School of Medicine, 143 Shimokasuya, Isehara, Kanagawa 259-1193, Japan
[c] Department of Microbiology, Mie University Graduate School of Medicine, 2-174 Edobashi, Tsu, Mie 514-8507, Japan
[d] Department of Hematology, Tokai University School of Medicine, 143 Shimokasuya, Isehara, Kanagawa 259-1193, Japan
[e] Division of Molecular Hematology, Kitasato University Graduate School of Medical Sciences, 1-15-1 Kitasato, Sagamihara, Kanagawa 228-8555, Japan

ARTICLE INFO

Article history:
Received 16 October 2009
Available online 22 October 2009

Keywords:
Myeloid leukemia
FLT3-ITD
Ara-C resistance
ENT1
HIF-1α

ABSTRACT

Fms-related tyrosine kinase 3-internal tandem duplications (*FLT3*-ITD) are strongly associated with the refractory nature of acute myeloid leukemia (AML) by the standard combined chemotherapy. FLT3-ITD-expressing murine and human myeloid cell lines, HF6/FLT3-ITD and K562/FLT3-ITD cells, respectively, were developed in order to clarify whether FLT3-ITD is involved in the resistance to cytotoxic agents in AML. Both of these cell lines were specifically resistant to the pyrimidine analogue cytosine arabinoside (ara-C), an essential agent for AML, accompanied by the downregulation of equilibrative nucleoside transporter 1 (ENT1), a transporter responsible for the cellular uptake of ara-C. The *ENT1* promoter activity and the cellular uptake of ara-C were reduced in K562/FLT3-ITD cells, and rescued by pretreating the cells with PKC412, a FLT3 inhibitor. In addition, the expression of *hypoxia inducible factor 1 alpha subunit* (*HIF1A*) transcripts was upregulated in K562/FLT3-ITD cells, and the induction of HIF-1α reduced the promoter activity of *ENT1* gene in K562 cells. Taken together, these findings suggest that FLT3-ITD specifically induces ara-C resistance in leukemic cells by the repression of ENT1 expression, possibly through the upregulation of HIF-1α, while also partially accounting for the poor prognosis of AML with FLT3-ITD due to resistance to the standard chemotherapy protocols which include ara-C.

Introduction

Acute myeloid leukemia (AML) is a group of neoplastic disorders characterized by the clonal accumulation of immature hematopoietic cells. It is thought to be caused by two types of genetic events: namely, class I mutations which induce cellular proliferation, and class II mutations which repress cellular differentiation [1].

One of the most frequent class I mutations is *fms-related tyrosine kinase 3*-internal tandem duplications (*FLT3*-ITD), which are observed in about 25% of AML cases [2–4]. Wild-type FLT3 product is one of class III receptor-type tyrosine kinases expressed in hematopoietic stem/progenitor cells, and it induces both their survival and proliferation through the activation of downstream targets, such as RAS/MAPK, PI3K/AKT and STAT5, when they are activated by binding to the FLT3 ligand [4,5]. A tandem repeat of several amino acids at the juxtamembrane domain in FLT3-ITD results in the constitutively active form of FLT3 through the autophosphorylation in a ligand-independent manner, which activates its unique pathways in addition to the targets of wild-type FLT3 [2–5]. *In vivo* analyses have confirmed that FLT3-ITD induces a myeloproliferative disease [6]. In addition, *FLT3*-ITD is also one of the most frequent poor prognostic factors in the standard combination chemotherapy, and is closely associated with a lower disease-free survival in AML with the normal karyotype [7,8].

The standard combination chemotherapy for the treatment of AML contains various kinds of cytotoxic agents which are designed to target the mechanisms involved in cellular proliferation: for example, anthracyclines inhibit DNA replication and RNA synthesis by intercalating the strands of nucleotides, pyrimidine analogues inhibit DNA polymerases through incorporation into DNA, and topoisomerase inhibitors inhibit DNA gyrases during cell division. Although aberrant signal transduction induced by FLT3-ITD is supposed to cause the survival advantage of AML cells during chemotherapy, the contribution of FLT3-ITD in the intrinsic resistance to specific cytotoxic agents and its underlying mechanisms are largely unknown [9].

We hypothesized that FLT3-ITD may influence the survival advantage during chemotherapy through directly inducing the resistance to cytotoxic agents. To this end, FLT3-ITD-expressing

* Corresponding author. Fax: +81 463 93 8607.
E-mail address: hmatsu@is.icc.u-tokai.ac.jp (H. Matsushita).

0006-291X/$ - see front matter © 2009 Elsevier Inc. All rights reserved.
doi:10.1016/j.bbrc.2009.10.094

myeloid cells were developed and their properties concerning the resistance to a specific cytotoxic agent were analyzed. The results identified a linkage between FLT3-ITD and resistance to ara-C, one of the essential agents in the current strategy of AML treatment, and its possible involvement in the mechanisms on the refractory nature of AML with FLT3-ITD are also herein discussed.

Materials and methods

Cells and reagents. Human leukemia cell line K562 cells were propagated in RPMI-1640 medium (Wako Pure Chemical Industries, Osaka, Japan) supplemented with heat-inactivated 10% fetal bovine serum (FBS). Murine myelomonocytic cell line HF6 cells were maintained in RPMI-1640 medium with 10% FBS and 20 ng/μl of murine IL-3 (Wako) [10]. Both of these cells were incubated at 37 °C in a humidified 5% CO_2. 1-β-D-arabinofuranosylcytosine (cytarabine, ara-C; Sigma–Aldrich, St. Louis, MO), doxorubicin (DOX; Wako), etoposide (VP-16; Wako), cisplatin (CDDP; Wako) and vincrisitine (VCR; Wako) were diluted with physiological saline solution to make 5, 2, 2, 2 and 20 mM stock solutions, respectively. Methotrexate (MTX; Wako) was diluted with RPMI-1640 (without FBS) to make a 20 mM stock solution. Idarubicn (IDR; Sigma–Aldrich) and trimetrexate (TMQ; Wako) were diluted with ethanol to make 0.5 and 2 mM stock solutions, respectively.

Transduction of vectors into the cells. The transduction of FLT3-ITD in HF6 cells was performed using retroviral infection. Briefly, pMYpuro-FLT3-ITD and its empty vector pMYpuro were transfected in PLAT-E cells (a generous gift from Dr. Toshio Kitamura, Institute of Medical Science, University of Tokyo, Tokyo, Japan) with FuGENE 6 (Roche Diagnostics, Basal, Switzerland) [10,11]. The culture supernatant was added to the plate coated with RetroNectin (Takara, Shiga, Japan) and incubated at 37 °C for 4 h. HF6 cells were then cultured on the plate at 37 °C for 48 h. The transduction of FLT3-ITD in K562 cells was performed using Nucleofector II system (Amaxa biosystems, Gaithersburg, MD), according to the manufacturer's protocol. FLT3-ITD- or pMYpuro-transduced HF6 and K562 cells, HF6/FLT3-ITD, HF6/pMY, K562/FLT3-ITD and K562/pMY cells, were purified with (2 μg/ml) of puromycin [11]. The transduction of pAcGFP1-C1 vector (Clontech, Mountain View, CA) expressing HIF-1α (pAcGFP1-C1/HIF-1α) into K562 cells was also performed using the Nucleofector II system.

Sensitivity to cytotoxic agents. Ten thousand cells per 200 μl were cultured under various concentrations of cytotoxic agents at 37 °C for 3 days. The IC_{50} (50% inhibiting concentration for cell growth) values for cytotoxic agents were determined by an MTT assay, as previously described [12]. The FLT3 inhibitor PKC412 (ALEXIS Biochemicals, Lausen, Switzerland) was added to the culture media, 48 h prior to the exposure to cytotoxic agents at IC_{20} (0.45, 0.31, 0.55 and 0.51 μM for K562/pMY and FLT3-ITD cells, HF6/pMY and FLT3-ITD cells, respectively).

Immunoprecipitation and a Western blot analysis. The cell pellets were suspended in the lysis buffer (50 mM Tris–HCl, 0.5 mM PHSF, 2 mM $CaCl_2$, 1% Triton X-100 with PH 7.4) with proteinase inhibitor (Complete, Roche Diagnostics) to obtain total cellular protein. Immunoprecipitation was carried out at 4 °C for 2 h by adding 10 μg of anti-FLT3 antibody (C-20, Santa Cruz biotechnology, Santa Cruz, CA) and protein A-Sepharose beads (GE Healthcare, Buckinghamshire, UK). Bound proteins were extracted using the elution buffer (0.58% acetic acid, 0.15 M NaCl) for SDS–polyacrylamide gel electrophoresis (SDS–PAGE). Equal amounts of the total cellular protein were separated by SDS–PAGE for direct Western blotting. The separated proteins on the gels were electronically transferred to polyvinylidene difluoride (PVDF) membrane. After blocking buffer (3% BSA and 0.1% NaN_3 in PBS) for 1 h at room temperature, the membrane was incubated with anti-phospho-tyrosine antibody (P-Tyr-102, Cell Signalling, Danvers, MA), anti-FLT3 or anti-β-actin antibody (Sigma–Aldrich) overnight at 4 °C. The ECL plus Western Blotting Detection System (GE Healthcare) was used for the detection of specific signals from proteins.

Reverse transcription (RT), polymerase chain reaction (PCR), and real-time PCR. Total RNA was extracted from cultured cells with ISOGEN (Nippon gene, Toyama, Japan). The cDNA was generated from 1 μg of total RNA using M-MLV Reverse Transcriptase kit (Invitrogen, Carlsbad, CA). PCR was performed in 25 μl of the final incubation volume using Ex Taq (Takara). Real-time PCR was performed using SYBR Premix Ex Taq II (Takara) and LightCycler (Roche Diagnostics), according to the manufacturer's protocol. RNA content was measured relative to that of *beta-actin* (*ACTB*) in K562 cells and *glyceraldehyde-3-phosphate dehydrogenase* (*Gapdh*) in HF6 cells, respectively. All the samples were independently analyzed at least three times for each gene. The sequences of the primer sets were as follows: human *equilibrative nucleoside transporter 1* (*ENT1*)-forward: 5′-CTCTCAGTGCCATCTTCAAC-3′, human *ENT1*-reverse: 5′-CAGAAACACCAGCAGGATGG-3′; murine *Ent1*-forward: 5′-ACTCTGTGTCCAGCTCTACC-3′, murine *Ent1*-reverse: 5′-ACTGGTTGTCATGGCTCCAG-3′; human *hypoxia inducible factor 1 alpha subunit* (*HIF1A*)-forward: 5′-TCTCCATCTCCTACCCACATAC-3′, human *HIF1A*-reverse: 5′-CTCCTTTTCCTGCTCTCTGTTTGG-3′; murine *deoxycytidine kinase* (*Dck*)-forward: 5′-GGACCCGCATCAAGAAGATC-3′, murine *Dck*-reverse: 5′-CTTGAGTGCTCTGCACGTTG-3′; murine *cytidine deaminase* (*Cda*)-forward: 5′-GTTCATCTCTCC CTGTGGAG-3′, murine *Cda*-reverse: 5′-GTCTTCAGGTCCAAACGAG G-3′. The PCR primer sets for human *FLT3* [13], *DCK* [14], *multidrug resistance 1* (*MDR1*) [12], *ACTB* [15], and murine *Gapdh* [10] were described previously.

Luciferase assay. A luciferase reporter construct was generated by inserting the DNA fragment of *ENT1* promoter region (2880–3990 base pairs from GenBank Accession No. AF495730.1) into pGL4.10 luciferase reporter vector (Promega, Madison, WI). The transduction of the construct was performed with Nucleofector II system using 1×10^6 cells and 2 μg of the plasmids. Luciferase activity was measured with the Luciferase Reporter Assay System (Promega) using a Turner Designs TD-20/20 luminometer (Promega).

Transport studies. One million exponentially growing cells were suspended in 1 ml of PBS containing 10 mM glucose and 2 mM glutamine for 15 min [15], followed by addition of ^{3}H-ara-C (Cytosine-β-D-arabinofuranoside, [5-^{3}H]; Moravek Biochemicals, Brea, CA; final concentration, 200 nM). The cell suspension was incubated at 37 °C for 10, 30 and 60 min. The cell pellets were digested with 105 μl of 1 N NaOH, and neutralized by addition of 105 μl of 1 N HCl. The cell-associated radioactivity was measured by the liquid scintillation analyzer (Perkin–Elmer, Waltham, MA).

Results

Generation of FLT3-ITD-expressing myeloid cells

IL-3-dependent HF6 cells from a mouse and K562 cells from a human were used for the generation of the myeloid cells expressing FLT3-ITD because of their high transduction efficiency (39% in HF6 cells by retroviral infection and 86% in K562 cells by electroporation, respectively). The expression of *FLT3*-ITD mRNA in HF6/FLT3-ITD and K562/FLT3-ITD cells was confirmed by RT-PCR (Fig. 1A). In HF6/FLT3-ITD cells, the expression of FLT3-ITD product was also confirmed by Western blot analysis (Fig. 1B). The tyrosine-residues were autophosphorylated, as expected (Fig. 1C), resulting in IL-3-independent proliferation of HF6/FLT3-ITD cells (Fig. 1D), as previously described [11].

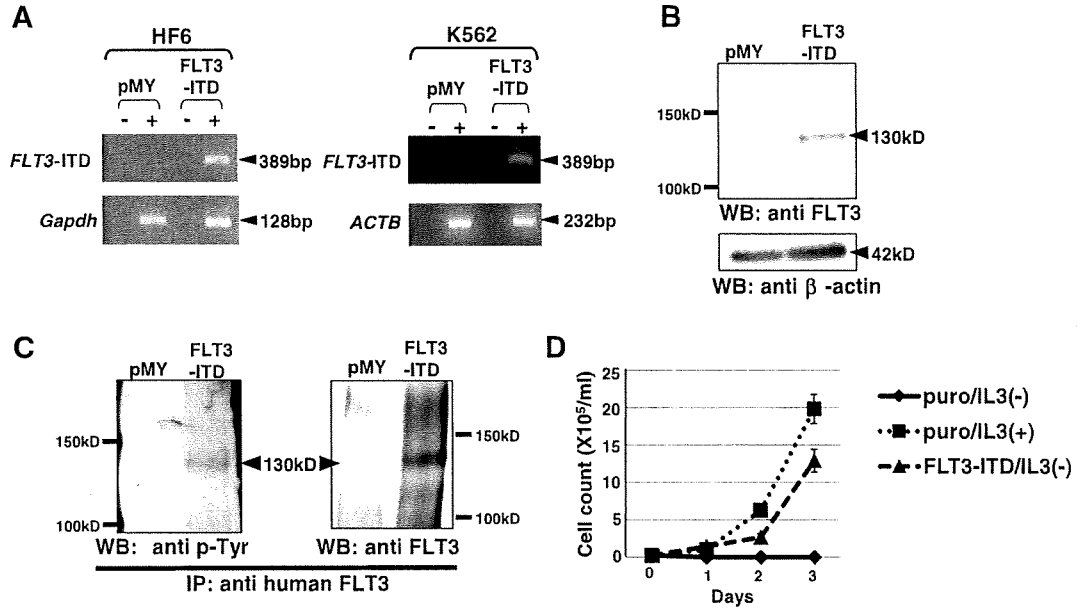

Fig. 1. Generation of FLT3-ITD-expressing myeloid cells. (A) The expression of *FLT3*-ITD transcript in HF6/FLT3-ITD and K562/FLT3-ITD cells. (B) The expression of FLT3-ITD product in HF6/FLT3-ITD cells. The major product at 130 kDa is indicated. (C) FLT3-ITD product was phosphorylated in HF6/FLT3-ITD cells. Immunoprecipitation was performed with anti-FLT3 antibodies, followed by a Western blot analysis using anti-phospho-tyrosine or anti-FLT3 antibody. (D) FLT3-ITD induced IL-3 independent-growth in HF6 cells. The cell numbers of HF6/FLT3-ITD and HF6/pMY cells cultured with or without murine IL-3 were analyzed.

FLT3-ITD specifically induced ara-C resistance in myeloid cells

These cells were exposed to several kinds of cytotoxic agents including a pyrimidine analogue (ara-C), anti-folates (MTX, TMQ), anthracyclines (DOX, IDR), a topoisomerase inhibitor (VP-16), a platinum-based agent (CDDP) and a vinca alkaloid (VCR). The IC_{50} for each cytotoxic agent was calculated from the cellular proliferation rates at their various concentrations. HF6/FLT3-ITD and K562/FLT3-ITD cells showed resistance to ara-C by 3.7- and 9.6-fold, as compared with empty vector-transduced HF6/pMY and K562/pMY cells, respectively. When these FLT3-ITD-expressing cells were pretreated with FLT3 inhibitor PKC412, the resistance to ara-C was completely reversed. In contrast, the expression of FLT3-ITD did not affect the IC_{50} values for all the other tested agents in both of HF6 and K562 cells, thus suggesting the specific resistance to ara-C induced by FLT3-ITD (Table 1).

Reduced expression of ENT1 and ara-C uptake in FLT3-ITD-expressing myeloid cells

Ara-C resistance has been previously shown to be induced in leukemic cells by an alteration of the expression and function of the genes and their products related to the cellular metabolism of ara-C; ENT1 is responsible for the cellular uptake of ara-C [16,17], DCK phosphorylates ara-C to form an active metabolite ara-C triphosphate (ara-CTP) [18,19], and CDA deaminates ara-C to form the inactive metabolite ara-U [20,21]. The expression of these genes was analyzed by real-time RT-PCR to identify the mechanisms for ara-C resistance in HF6/FLT3-ITD cells. No differences in the expression of *Dck* and *Cda* mRNA were observed between the FLT3-ITD- and control vector (pMYpuro)-transduced cells. In contrast, the expression of *Ent1* mRNA was decreased in HF6/FLT3-ITD cells. The reduced expression of *Ent1* mRNA in HF6/FLT3-ITD cells was reversed when the cells were pre-exposed to PKC412 (Fig. 2A and data not shown). The decrease of ENT1 product was confirmed in HF6/FLT3-ITD cells by a Western blot analysis (Fig. 2B). Similar results were obtained, when the expression of these transcripts was compared in K562/FLT3-ITD and K562/pMY cells (data not shown).

Meanwhile, the expression of *MDR1* transcript, which encodes *p*-glycoprotein functioning as an efflux pump for cytotoxic agents including anthracyclines and vinca alkaloids, was not induced in K562/FLT3-ITD cells, as evaluated by real-time RT-PCR (data not shown) [22].

The luciferase reporter harboring the promoter region of *ENT1* gene was transduced into K562/FLT3-ITD and K562/pMY cells and the promoter activity of *ENT1* was measured by a luciferase assay. The plasmids were similarly transduced into both of the cells using a GFP-expressing plasmid, pAcGFP1-C1. The activity of the *ENT1* promoter was reduced in K562/FLT3-ITD in comparison to K562/pMY cells (0.42-fold), and rescued by pre-exposure to PKC412 (1.1-fold; Fig. 2C).

The intracellular uptake of ara-C in K562/FLT3-ITD and K562/pMY cells was analyzed. The transmembrane transport of ^{3}H-ara-C was dependent on the incubation time in all of these cells. It was consistently reduced in K562/FLT3-ITD cells at each time point, in comparison to K562/pMY cells (0.43-fold at 60 min). In addition, pre-exposure of K562/FLT3-ITD cells to PKC412 rescued the cellular uptake of ara-C (1.21-fold at 60 min; Fig. 2D). These findings were consistent with the reduced expression of *ENT1* induced by FLT3-ITD.

FLT3-ITD inhibited the ENT1 expression through upregulation of HIF-1α

The promoter region of ENT1 has the presumed binding sites of several transcriptional factors including hypoxia inducible factor 1 (HIF-1), which is thought to negatively regulate the expression of ENT1 [23]. HIF-1 heterodimer complex is composed of α and β subunits, and its function is regulated by the dose of HIF-1α in hypoxic status [24,25]. The expression of *HIF1A* was examined in K562/FLT3-ITD and K562/pMY cells using real-time RT-PCR. The *HIF1A* mRNA in K562/FLT3-ITD cells was increased by 6.2-fold in comparison to K562/pMY cells (Fig. 3A). HIF-1α-transduced K562 (K562/

Table 1
IC_{50} values for various cytotoxic agents in FLT3-ITD-transduced myeloid cells.

Reagent		PKC412 treatment	IC_{50} (μM)		Relative resistance (A/B)[a]
			(A) FLT3-ITD-transduced	(B) pMYpuro-transduced	
HF6	Ara-C	No	0.14 ± 0.031	0.038 ± 0.0032	3.7
		Yes	0.030 ± 0.015	0.030 ± 0.0032	1.0
	MTX	No	0.0037 ± 0.00042	0.0035 ± 0.00051	1.1
	TMQ	No	0.0036 ± 0.00081	0.0038 ± 0.00011	0.95
	DOX	No	0.0063 ± 0.0013	0.0061 ± 0.00023	0.95
	VP-16	No	0.061 ± 0.0062	0.054 ± 0.011	1.1
	CDDP	No	0.76 ± 0.11	0.65 ± 0.10	1.2
K562	Ara-C	No	1.6 ± 0.31	0.17 ± 0.035	9.6
		Yes	0.18 ± 0.031	0.18 ± 0.035	1.0
	MTX	No	0.0088 ± 0.00072	0.0094 ± 0.00054	0.94
	TMQ	No	0.0082 ± 0.0011	0.0087 ± 0.00083	0.94
	DOX	No	0.095 ± 0.0064	0.075 ± 0.049	1.3
	IDR	No	0.053 ± 0.0021	0.056 ± 0.0014	0.95
	VP-16	No	2.6 ± 0.21	3.2 ± 0.56	0.80
	VCR	No	0.0093 ± 0.0018	0.011 ± 0.0016	0.85

[a] They were calculated as the ratio of the IC_{50} for each cytotoxic agent from FLT3-ITD-transduced cells to those from pMYpuro-transduced cells.

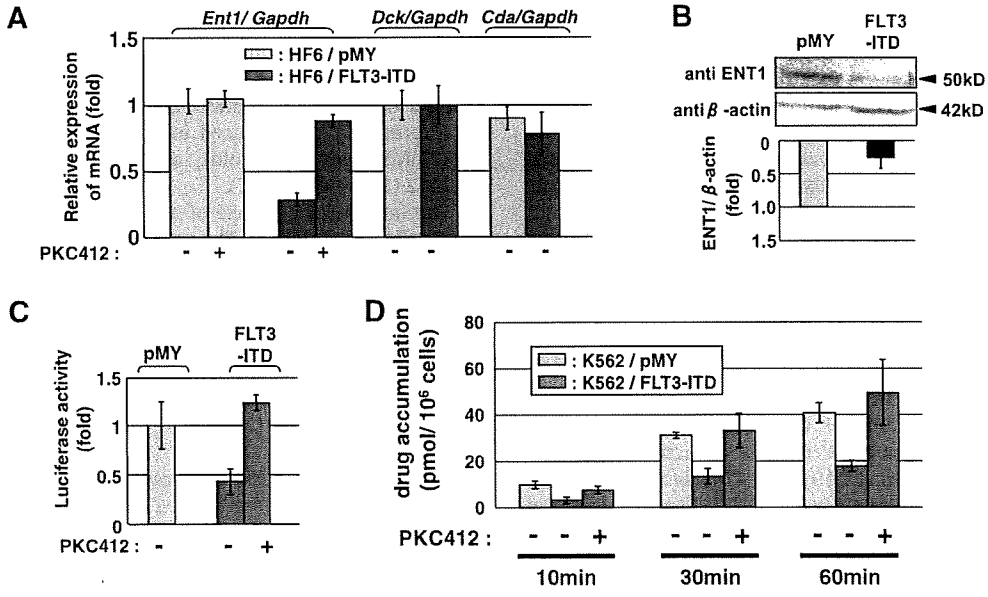

Fig. 2. Reduced ENT1 expression and ara-C uptake in FLT3-ITD-expressing myeloid cells. (A) The expression of *Ent1*, *Dck* and *Cda* mRNA in HF6/FLT3-ITD cells. The cells were pretreated with PKC412 for 48 h followed by exposure to ara-C. The content of each transcript was expressed as its relative ratios to that of murine *Gapdh*. The relative ratios in regard to the data from the HF6/pMY without pretreatment of PKC412 are presented. (B) The expression of ENT1 product in HF6/FLT3-ITD cells. The ratio of ENT1/β-actin was assessed by densitometry and presented the histogram at the bottom. The value obtained from the HF6/pMY cells is expressed arbitrarily as 1. (C) The activity of the *ENT1* promoter in K562/FLT3-ITD cells evaluated by a luciferase assay. The cells were pretreated with PKC412 for 48 h followed by the transduction of a reporter plasmid. The relative ratios with regard to the data from K562/pMY cells are presented. (D) The intracellular transport of ara-C in K562/FLT3-ITD and K562/pMY cells. One million cells were incubated in the presence of 200 nmol/l of [^{3}H]-ara-C with or without the pretreatment of PKC412. The intracellular accumulation of [^{3}H]-ara-C measured under each condition is presented.

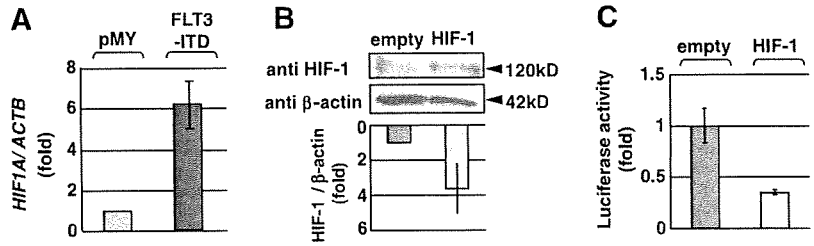

Fig. 3. FLT3-ITD inhibited the ENT1 expression through upregulation of HIF-1α. (A) The expression of *HIF1A* transcripts in K562/FLT3-ITD cells. The content of *HIF1A* transcript was expressed as its relative ratios to that of *ACTB*. The relative ratio in regard to the data from the K562/empty is presented as fold. (B) The expression of HIF-1α products in K562/HIF-1α cells. The ratio of HIF-1α/β-actin was assessed by densitometry and presented the histogram at the bottom. The value obtained from the K562/empty cells is expressed arbitrarily as 1. (C) The activity of the *ENT1* promoter in K562/HIF-1α cells evaluated by a luciferase assay. The relative ratio in regard to the data from the K562/pAcGFP1-C1 is presented.

HIF-1α) cells were generated. The induced expression of the HIF-1α product in K562/HIF-1α cells was confirmed by a Western blot analysis (Fig. 3B). A luciferase assay showed that the promoter activity of *ENT1* gene was reduced in K562/HIF-1α cells in comparison to K562/empty cells (0.35-fold; Fig. 3C). These findings suggested that the FLT3-ITD induced the expression of HIF-1α which suppressed the promoter activity of *ENT1* gene in the myeloid cells.

Discussion

Most of previous studies on the chemotherapy-resistance in AML have been performed using cultured cells after long-term exposure to cytotoxic agents and elucidated the mechanisms of acquired resistances. This study demonstrated that the FLT3-ITD rendered the myeloid cells specifically resistant to ara-C by the downregulation of ENT1, which may have been caused by HIF-1α induction. This is the first report indicating a direct relationship between FLT3-ITD and resistance to a specific cytotoxic agent through transcriptional alterations.

Ara-C is one of the crucial agents in the current strategy of AML treatment. The treatment regimen using ara-C in combination with other cytotoxic agents including anthracyclines is a standard protocol of induction therapy, and a regimen with high-dose ara-C is used as a post-remission therapy for good-risk AML [26,27]. On the other hand, AML with *FLT3*-ITD is recognized as a subgroup with a poor risk, and these patients often relapse or develop refractory disease [2,3]. A major possible mechanism is presumed that the cellular proliferation and survival induced by FLT3-ITD may lead to overcoming cytotoxicity of the chemotherapy. Other than numerous proteins related to signal transduction, there have been reported several downstream target molecules of FLT3-ITD: Pim-1, a proto-oncogene, protects hematopoietic cells from apoptosis [28,29]. RAD51 participates in DNA repair with double strand breaks [30]. This study found that FLT3-ITD induced resistance against ara-C by downregulation of ENT1 resulting reduced cellular uptake of ara-C. The agent-specific resistance has been usually observed in acquired resistance and the cause has been explained by cellular-pharmacological mechanisms including the alteration of transport, target and metabolism of drugs. The current finding therefore suggests that such mechanisms also possibly contribute to the development of intrinsic resistance in association with altered signal transduction, when such resistance is specific to a certain agent.

This study also shows the potential contribution of HIF-1α to FLT3-ITD-induced ara-C resistance. HIF-1α is upregulated at low oxygen concentrations for the adaptation to hypoxic conditions, but is often aberrantly expressed in tumor cells for the proliferation and survival dominance even under normoxic conditions [24,25]. HIF-1α is activated by the phosphatidylinositol 3-kinase (PI3K)/AKT and mitogen-activated protein kinase (MAPK/ERK) signal transduction pathways, both of which are triggered by FLT3 activation [4], and induces the expression of *MDR1* mRNA [31]. This is supported by a recent report from Oveland et al., stating that the downregulation of FLT3 signals in AML cells enhanced the sensitivity to a semi-synthetic anthracycline IDR, another crucial agent in combination chemotherapy for AML [32]. This study, however, showed that FLT3-ITD induced neither the expression of *MDR1*, nor the specific resistance to anthracycline analogues, IDR and DOX. This differential effect of FLT3-ITD on the chemotherapy-sensitivity might have been derived from the difference between FLT3 and FLT3-ITD signal transduction, although it could be possibly due to different experimental designs including types of cells used in the study.

There have so far been few reports regarding the role of FLT3-ITD in chemotherapy-resistance. However, these two studies, including Oveland et al.'s and this study proposed the idea that the inhibition of FLT3 signals would enhance the sensitivity of ara-C and IDR, the key agents in AML treatment [32]. These may support the theoretical relevance for the clinical use of FLT3 inhibitors in the treatment of AML with FLT3-ITD. The efficacy of FLT3 inhibitors in the treatment of AML with FLT3-ITD, in combination with cytotoxic agents, is currently under evaluation in several clinical trials [2–4]. Although the FLT3 inhibitors are basically expected to inhibit the cellular proliferation through the downregulation of FLT3 signals, they would also operate as a chemo-sensitizer in these trials. Accordingly, it is possible that the FLT3 inhibitors should be administered prior to the administration of other cytotoxic agents.

In summary, the findings in this study suggest that FLT3-ITD specifically induces ara-C resistance in myeloid leukemia cells through the repression of ENT1 expression which may be caused by HIF-1α, thereby demonstrating that FLT3-ITD is involved in the intrinsic resistance to a specific agent in AML through aberrant signal transduction. Understanding the mechanisms of FLT3-ITD-induced chemotherapy-resistance in AML will therefore contribute to the development of novel therapeutic approaches including FLT3 inhibitors, and thereby improve the prognosis of this subtype of AML.

Acknowledgment

This study was supported in part by Tokai University School of Medicine Research Aid.

References

[1] L.M. Kelly, D.G. Gilliland, Genetics of myeloid leukemias, Annu. Rev. Genom. Hum. Genet. 3 (2002) 179–198.
[2] D. Small, FLT3 mutations: biology and treatment, Hematol. Am. Soc. Hematol. Educ. Program (2006) 178–184.

[3] H. Kiyoi, T. Naoe, Biology clinical relevance and molecularly targeted therapy in acute leukemia with FLT3 mutation, Int. J. Hematol. 83 (2006) 301–308.
[4] D.L. Stirewalt, J.P. Radich, The role of FLT3 in haematopoietic malignancies, Nat. Rev. Cancer 3 (2003) 650–665.
[5] J.T. Reilly, Class III receptor tyrosine kinases: role in leukaemogenesis, Br. J. Haematol. 116 (2002) 744–757.
[6] L.M. Kelly, Q. Liu, J.L. Kutok, I.R. Williams, C.L. Boulton, D.G. Gilliland, FLT3 internal tandem duplication mutations associated with human acute myeloid leukemias induce myeloproliferative disease in a murine bone marrow transplant model, Blood 99 (2002) 310–318.
[7] A. Renneville, N. Boissel, N. Gachard, D. Naguib, C. Bastard, S. de Botton, O. Nibourel, C. Pautas, O. Reman, X. Thomas, C. Gardin, C. Terré, S. Castaigne, C. Preudhomme, H. Dombret, The favorable impact of CEBPA mutations in patients with acute myeloid leukemia is only observed in the absence of associated cytogenetic abnormalities and FLT3 internal duplication, Blood 113 (2009) 5090–5093.
[8] R.F. Schlenk, K. Döhner, J. Krauter, S. Fröhling, A. Corbacioglu, L. Bullinger, M. Habdank, D. Späth, M. Morgan, A. Benner, B. Schlegelberger, G. Heil, A. Ganser, H. Döhner, German–Austrian Acute Myeloid Leukemia Study Group, Mutations and treatment outcome in cytogenetically normal acute myeloid leukemia, N. Engl. J. Med. 358 (2008) 1909–1918.
[9] G.D. Kruh, Introduction to resistance to anticancer agents, Oncogene 22 (2003) 7262–7264.
[10] H. Matsushita, H. Nakajima, Y. Nakamura, H. Tsukamoto, Y. Tanaka, G. Jin, M. Yabe, S. Asai, R. Ono, T. Nosaka, K. Sugita, A. Morimoto, Y. Hayashi, T. Hotta, K. Ando, H. Miyachi, C/EBPalpha and C/EBPepsilon induce the monocytic differentiation of myelomonocytic cells with the MLL-chimeric fusion gene, Oncogene 27 (2008) 6749–6760.
[11] R. Ono, H. Nakajima, K. Ozaki, H. Kumagai, T. Kawashima, T. Taki, T. Kitamura, Y. Hayashi, T. Nosaka, Dimerization of MLL fusion proteins and FLT3 activation synergize to induce multiple-lineage leukemogenesis, J. Clin. Invest. 115 (2005) 919–929.
[12] H. Miyachi, L. Ma, Y. Takemura, H. Kobayashi, I. Hirahara, H. Sonehara, Y. Ando, Microsatellite instability and clonal heterogeneity of MDR1 messenger RNA expression in trimetrexate-resistant human leukemia MOLT-3 cells developed in thymidine, Int. J. Cancer 82 (1999) 63–69.
[13] S. Fröhling, R.F. Schlenk, J. Breitruck, A. Benner, S. Kreitmeier, K. Tobis, H. Döhner, K. Döhner, Prognostic significance of activating FLT3 mutations in younger adults (16–60 years) with acute myeloid leukemia and normal cytogenetics: a study of the AML Study Group Ulm, Blood 100 (2002) 4372–4380.
[14] J. Cai, V.L. Damaraju, N. Groulx, D. Mowles, Y. Peng, M.J. Robins, C.E. Cass, P. Gros, Two distinct molecular mechanisms underlying cytarabine resistance in human leukemic cells, Cancer Res. 68 (2008) 2349–2357.
[15] T. Nakanishi, J.E. Karp, M. Tan, L.A. Doyle, T. Peters, W. Yang, D. Wei, D.D. Ross, Quantitative analysis of breast cancer resistance protein and cellular resistance to flavopiridol in acute leukemia patients, Clin. Cancer Res. 9 (2003) 3320–3328.
[16] E.I. Zimmerman, M. Huang, A.V. Leisewitz, Y. Wang, J. Yang, L.M. Graves, Identification of a novel point mutation in ENT1 that confers resistance to Ara-C in human T cell leukemia CCRF-CEM cells, FEBS Lett. 583 (2009) 425–429.
[17] K. Takagaki, S. Katsuma, Y. Kaminishi, T. Horio, S. Nakagawa, T. Tanaka, T. Ohgi, J. Yano, Gene-expression profiling reveals down-regulation of equilibrative nucleoside transporter 1 (ENT1) in Ara-C-resistant CCRF-CEM-derived cells, J. Biochem. 136 (2004) 733–740.
[18] J.H. Song, S.H. Kim, S.H. Kweon, T.H. Lee, H.J. Kim, H.J. Kim, T.S. Kim, Defective expression of deoxycytidine kinase in cytarabine-resistant acute myeloid leukemia cells, Int. J. Oncol. 34 (2009) 1165–1171.
[19] T. Yamauchi, E. Negoro, S. Kishi, K. Takagi, A. Yoshida, Y. Urasaki, H. Iwasaki, T. Ueda, Intracellular cytarabine triphosphate production correlates to deoxycytidine kinase/cytosolic 5′-nucleotidase II expression ratio in primary acute myeloid leukemia cells, Biochem. Pharmacol. 77 (2009) 1780–1786.
[20] K. Yusa, T. Oh-hara, S. Tsukahara, T. Tsuruo, Human immunodeficiency virus type 1 induces 1-beta-D-arabinofuranosylcytosine resistance in human H9 cell line, J. Biol. Chem. 267 (1992) 16848–16850.
[21] C.D. Steuart, P.J. Burke, Cytidine deaminase and the development of resistance to arabinosyl cytosine, Nat. New Biol. 233 (1971) 109–110.
[22] D. Mahadevan, A.F. List, Targeting the multidrug resistance-1 transporter in AML: molecular regulation and therapeutic strategies, Blood 104 (2004) 1940–1951.
[23] H.K. Eltzschig, P. Abdulla, E. Hoffman, K.E. Hamilton, D. Daniels, C. Schönfeld, M. Löffler, G. Reyes, M. Duszenko, J. Karhausen, A. Robinson, K.A. Westerman, I.R. Coe, S.P. Colgan, HIF-1-dependent repression of equilibrative nucleoside transporter (ENT) in hypoxia, J. Exp. Med. 202 (2005) 1493–1505.
[24] M.C. Brahimi-Horn, J. Pouysségur, HIF at a glance, J. Cell Sci. 122 (2009) 1055–1057.
[25] G.L. Semenza, Targeting HIF-1 for cancer therapy, Nat. Rev. Cancer 3 (2003) 721–732.
[26] C.D. Bloomfield, D. Lawrence, J.C. Byrd, A. Carroll, M.J. Pettenati, R. Tantravahi, S.R. Patil, F.R. Davey, D.T. Berg, C.A. Schiffer, D.C. Arthur, R.J. Mayer, Frequency of prolonged remission duration after high-dose cytarabine intensification in acute myeloid leukemia varies by cytogenetic subtype, Cancer Res. 58 (1998) 4173–4179.
[27] M.S. Tallman, D.G. Gilliland, J.M. Rowe, Drug therapy for acute myeloid leukemia, Blood 106 (2005) 1154–1163.
[28] K.T. Kim, M. Levis, D. Small, Constitutively activated FLT3 phosphorylates BAD partially through pim-1, Br. J. Haematol. 134 (2006) 500–509.
[29] T. Nosaka, T. Kitamura, Pim-1 expression is sufficient to induce cytokine independence in murine hematopoietic cells, but is dispensable for BCR-ABL-mediated transformation, Exp. Hematol. 30 (2002) 697–702.
[30] C.H. Seedhouse, H.M. Hunter, B. Lloyd-Lewis, A.M. Massip, M. Pallis, G.I. Carter, M. Grundy, S. Shang, N.H. Russell, DNA repair contributes to the drug-resistant phenotype of primary acute myeloid leukaemia cells with FLT3 internal tandem duplications and is reversed by the FLT3 inhibitor PKC412, Leukemia 20 (2006) 2130–2136.
[31] K. Kohno, T. Uchiumi, I. Niina, T. Wakasugi, T. Igarashi, Y. Momii, T. Yoshida, K. Matsuo, N. Miyamoto, H. Izumi, Transcription factors and drug resistance, Eur. J. Cancer 41 (2005) 2577–2586.
[32] E. Oveland, B.T. Gjertsen, L. Wergeland, F. Selheim, K.E. Fladmark, R. Hovland, Ligand-induced Flt3-downregulation modulates cell death associated proteins and enhances chemosensitivity to idarubicin in THP-1 acute myeloid leukemia cells, Leuk. Res. 33 (2009) 276–287.

Leukemia (2009) 23, 2197–2209

www.nature.com/leu

LEADING ARTICLE

Mixed-lineage-leukemia (*MLL*) fusion protein collaborates with Ras to induce acute leukemia through aberrant *Hox* expression and Raf activation

R Ono[1,2,3], H Kumagai[1], H Nakajima[4,5], A Hishiya[1,2], T Taki[6], K Horikawa[7], K Takatsu[7,8], T Satoh[9], Y Hayashi[10], T Kitamura[2] and T Nosaka[1,2,3]

[1]*Division of Hematopoietic Factors, The Institute of Medical Science, The University of Tokyo, Tokyo, Japan;* [2]*Division of Cellular Therapy, The Institute of Medical Science, The University of Tokyo, Tokyo, Japan;* [3]*Department of Microbiology and Molecular Genetics, Mie University Graduate School of Medicine, Mie, Japan;* [4]*Center of Excellence, The Institute of Medical Science, The University of Tokyo, Tokyo, Japan;* [5]*Division of Hematology, Department of Internal Medicine, Keio University School of Medicine, Tokyo, Japan;* [6]*Department of Molecular Laboratory Medicine, Kyoto Prefectural University of Medicine Graduate School of Medical Science, Kamigyo-ku, Kyoto, Japan;* [7]*Department of Immunology, The Institute of Medical Science, The University of Tokyo, Tokyo, Japan;* [8]*Department of Immunobiology and Pharmaceutical Genetics, Graduate School of Medicine and Pharmaceutical Sciences, University of Toyama, Toyama, Japan;* [9]*Division of Molecular Biology, Department of Biochemistry and Molecular Biology, Kobe University Graduate School of Medicine, Kobe, Japan and* [10]*Gunma Children's Medical Center, Gunma, Japan*

Mixed-lineage-leukemia* (*MLL*) fusion oncogenes are closely involved in infant acute leukemia, which is frequently accompanied by mutations or overexpression of *FMS-like receptor tyrosine kinase 3* (*FLT3*). Earlier studies have shown that *MLL* fusion proteins induced acute leukemia together with another mutation, such as an *FLT3* mutant, in mouse models. However, little has hitherto been elucidated regarding the molecular mechanism of the cooperativity in leukemogenesis. Using murine model systems of the *MLL*-fusion-mediated leukemogenesis leading to oncogenic transformation *in vitro* and acute leukemia *in vivo*, this study characterized the molecular network in the cooperative leukemogenesis. This research revealed that *MLL* fusion proteins cooperated with activation of Ras *in vivo*, which was substitutable for Raf *in vitro*, synergistically, but not with activation of signal transducer and activator of transcription 5 (STAT5), to induce acute leukemia *in vivo* as well as oncogenic transformation *in vitro*. Furthermore, *Hoxa9*, one of the *MLL*-targeted critical molecules, and activation of Ras *in vivo*, which was replaceable with Raf *in vitro*, were identified as fundamental components sufficient for mimicking *MLL*-fusion-mediated leukemogenesis. These findings suggest that the molecular crosstalk between aberrant expression of *Hox* molecule(s) and activated Raf may have a key role in the *MLL*-fusion-mediated-leukemogenesis, and may thus help develop the novel molecularly targeted therapy against *MLL*-related leukemia.

Leukemia (2009) **23,** 2197–2209; doi:10.1038/leu.2009.177; published online 27 August 2009
Keywords: MLL; Ras; MAP kinase; leukemogenesis

Introduction

Multistep oncogenesis has been suggested in malignancy by the observation of more than two heterogeneous genetic and/or epigenetic lesions.[1] In leukemogenesis, recurring chromosomal translocations are frequently found in hematological malignancies, which sometimes coincide with subtle but critical genetic mutations leading to functional aberration.[2–4] Earlier studies showed that many of the translocation target genes are transcription factors involved in hematopoietic differentiation and/or self-renewal, whereas coincident mutations often occur on the genes involved in cell proliferation.[4] These results lead to a hypothetical model of leukemogenesis in which these two kinds of genetic alterations may cooperate to induce acute leukemia. This concept has been recently exemplified in experimental models using combinations of fusion genes, including *mixed-lineage leukemia* (*MLL*, also called *ALL1* or *HRX*) or *AML1* fusion genes, and other coincident genetic mutations.[5–9]

MLL is a proto-oncogene that is rearranged in human acute leukemia with chromosome 11 band q23 (11q23) translocation,[10,11] encoding a histone methyltransferase that assembles in a chromatin-modifying supercomplex.[12] Meanwhile, *MLL* fusion gene leads to leukemogenesis through several *HOX* genes directly transactivated by *MLL* fusion protein itself.[4,11,13,14] It is noteworthy that most of the genetically engineered mice carrying the *MLL* fusion developed hematological malignancy after a long latency, suggesting that secondary genotoxic stress is required to develop overt acute leukemia.[15–18] An earlier study presented direct evidence that *MLL* fusion proteins induced myeloproliferative disease (MPD) with a long latency, and caused acute leukemia with a short latency together with a coincident mutation of *FMS-like tyrosine kinase 3* (*FLT3*).[6]

Recent studies revealed that genetic alterations, including *FLT3*, *NRAS* (neuroblastoma RAS viral (v-ras) oncogene homolog) and *KRAS* (v-Ki-ras2 Kirsten rat sarcoma viral oncogene homolog), are frequently accompanied by 11q23 translocation.[19,20] *FLT3* is a receptor tyrosine kinase involved in leukemogenesis and normal hematopoiesis.[21] The mutations of *FLT3* are mainly classified into length mutations such as internal tandem duplication (ITD) of the juxtamembrane domain, and point mutations within the activation loop of the second tyrosine kinase domain (TKD).[21] Interestingly, *FLT3*-TKD, as well as overexpression of the wild type of FLT3, is found to be frequently associated with infant acute lymphoid leukemia (ALL), with rearrangements of *MLL*.[19,22] Both types of *FLT3* mutations result in a constitutive activation of *FLT3* kinase activity, followed by activation of signaling pathways, including signal transducer and activator of transcription 5 (STAT5) and Ras/Raf/mitogen-activated protein (MAP) kinase.[23,24] Both STAT5 and Ras/Raf/MAP kinase (MAPK) are involved in cellular

Correspondence: Dr T Nosaka, Department of Microbiology and Molecular Genetics, Mie University Graduate School of Medicine, 2-174 Edobashi, Tsu, Mie 514-8507, Japan.
E-mail: nosaka@doc.medic.mie-u.ac.jp
Received 1 October 2008; revised 17 July 2009; accepted 21 July 2009; published online 27 August 2009

proliferation, survival and differentiation.[25,26] Constitutively active mutants of Ras induce oncogenic transformation through activation of the MAPK cascade.[26] However, little has so far been elucidated regarding the molecular mechanism of collaboration in leukemogenesis.

To further clarify the molecular mechanism of *MLL*-fusion-mediated leukemogenesis, we focused on signal transduction associated with malignant transformation that collaborates with *MLL* fusion protein *in vitro*, and highlighted the contrastive roles of STAT5 and MAPK in leukemogenesis. Interestingly, comparative analyses suggested synergistic collaboration with activated Ras in *MLL*-fusion-mediated leukemogenesis, and also activation of Raf in malignant transformation *in vitro*, but not with STAT5 activation *in vivo* and *in vitro*. Thus, the activation of Ras/Raf/MAPK cascade may have an important role in multistep leukemogenesis with 11q23 translocations.

Materials and methods

Construction of the plasmids and retrovirus production

Fragments of murine constitutively active mutants of STAT5A (#2[27] and 1*6[28]) fused with a FLAG tag at the C-terminus, a coding region of human *NRAS*^{G12V} and *MLL-eleven nineteen leukemia* (*ENL*) short form[6] were inserted upstream of the internal ribosomal entry site (IRES)-enhanced green fluorescent protein (EGFP) cassette of pMYs-IRES-EGFP.[29] Fragments of coding regions of a wild type of *NRAS* and *NRAS*^{G12V} were inserted into pMXs-puro.[29] A fragment of murine *Hoxa9*[30] (a kind gift from Dr G Sauvageau) was inserted into pMXs-IRES-EGFP.[29] A fragment of a dominant negative mutant (dn) of STAT5A[23] was inserted upstream of the IRES-Kusabira-Orange (KO)[31] cassette of pMXs-IRES-KO, in which the EGFP cassette in pMXs-IRES-EGFP[29] was replaced with the KO cassette of phKO1-S1 (MBL, Nagoya, Japan). pMXs-neo-*MLL-SEPT6*,[6] pMY-FLT3-ITD-IRES-EGFP,[6] pMY-FLT3^{D835V}-IRES-EGFP[6] and pBabe-puro-Δ*Raf*-estrogen receptor (ER)[28] were described earlier. Retroviruses were harvested 48 h after transfection with each retroviral construct into PlatE cells[29] in which appropriate expression of the transgenes was confirmed by western blot analysis, as described earlier.[6]

Cells

An *MLL-SEPT6*-immortalized murine myelomonocytic cell line, HF6, was established through colony-replating assays using retroviral transduction with pMXs-neo-*MLL-SEPT6* as described earlier.[6] A *Hoxa9*-immortalized murine myelomonocytic cell line, A9G, was established through infection with retroviruses harboring *Hoxa9* in pMXs/IRES-EGFP[29] as reported earlier.[32] The HF6,[6] A9G and murine pro-B Ba/F3[28] cells were cultured in the presence of interleukin-3 (IL-3) (R&D Systems, Minneapolis, MN, USA). HF6 cells transduced with *FLT3* mutants were cultured in the same medium, except for the absence of IL-3. The expression levels of *FLT3* in these cells were evaluated using a phycoerythrin (PE)-conjugated anti-CD135 antibody, or an anti-mouse immunoglobulin G1,κ, as the isotype-matched control (BD Biosciences, San Diego, CA, USA) using fluorescence-activated cell sorting (FACS) Calibur (BD Biosciences) as described earlier.[33]

Immunoprecipitation and western blot analysis

Fifty million parental and additionally transduced HF6 cells, or 10 million parental and transduced Ba/F3 cells, were harvested in the lysis buffer, and the lysates were either suspended with 1 × sodium dodecyl sulfate sample buffer after immunoprecipitation using polyclonal anti-STAT5A antibody (L-20) (Santa Cruz Biotechnology, Santa Cruz, CA, USA) or directly mixed with an equal volume of 2 × sodium dodecyl sulfate sample buffer and then boiled, as described earlier.[25] In some experiments, the parental HF6 cells had been deprived of IL-3 8 h before harvest. Western blot analysis of each sample was performed using the polyclonal anti-STAT5A (L-20), monoclonal anti-phosphotyrosine (4G10) (Upstate Biotechnology, Lake Placid, NY, USA), polyclonal anti-extracellular signal-related kinase (ERK)1/2, monoclonal anti-phospho-ERK1/2 (E10) (Cell Signaling Technology, Danvers, MA, USA), monoclonal anti-α-tubulin (Sigma-Aldrich, St Louis, MO, USA), monoclonal anti-FLAG (M2), polyclonal anti-ERα (MC-20) and monoclonal anti-N-Ras (F155) (Santa Cruz Biotechnology) antibodies to probe membranes, as described earlier.[25]

Evaluation of cellular effects by inhibition of signal transduction in vitro

The response to the drug was evaluated as described earlier.[23] In brief, HF6 cells expressing the *FLT3* mutants (3×10^5) were infected with retroviruses harboring or not harboring the dnSTAT5A in pMXs-IRES-KO in the presence of polybrene, as described earlier.[6] Viable cell numbers were counted with standard Trypan blue staining, and the expression of the dnSTAT5A was monitored by assessment of KO positivity using the FL2 channel on the FACS Calibur, daily after infection. At 48 h after infection, to evaluate the status of phosphorylated STAT5, half a million of these cells were fixed with fixation buffer, permeablized with Perm Buffer III and analyzed with an Alexa Fluor 647-conjugated anti-phospho-STAT5 (Y694) (all from BD Biosciences) antibody, or the anti-mouse immunoglobulin G1,κ, as the isotype-matched control antibody, using the FL4 channel on the FACS Calibur, according to the manufacturer's recommendation. As controls, the parental HF6 cells with and without IL-3 stimulation after deprivation of IL-3 for 8 h were used. Meanwhile, these HF6 cells (1×10^4) were cultured for 72 h in 24-well plates in the presence of various concentrations of a MAPK kinase (MEK) inhibitor, U0126, or a PI3 kinase inhibitor, LY294002 (Calbiochem-Novabiochem, San Diego, CA, USA) and each vehicle control (ethanol for U0126 and dimethyl sulfoxide for LY294002). Viable cell numbers were counted with standard Trypan blue staining after each treatment, followed by calculation of the 50% inhibitory concentration (IC50) of each drug using a logistic regression model. To evaluate the inhibitory effect of U0126 on ERK1/2, five million of the cells were treated for 2 h, harvested and analyzed with the anti-ERK1/2 or the anti phospho-ERK1/2 antibody after western blotting.

Myeloid transformation assays in vitro

In a series of transformation assays, the acquisition of IL-3-independent proliferation was examined in IL-3-dependent cells. HF6 and Ba/F3 cells were infected with retroviruses harboring *NRAS*, *NRAS*^{G12V} or mock in pMXs-puro; Δ*Raf*-ER or mock in pBabe puro; and STAT5A1*6, STAT5A#2 or none (only GFP) in pMYs-IRES-EGFP, respectively, in the presence of polybrene, as described earlier.[6] A9G cells were also retrovirally transduced with *NRAS*, *NRAS*^{G12V} Δ*Raf*-ER or each mock in the same way. For puromycin selection, the transduced cells were cultured with 1 μg/ml of puromycin 24–96 h after infection, followed by propagation for 5 days in the absence of puromycin.

Next, 1×10^5 puromycin-resistant cells transduced with *NRAS*, *NRAS*^{G12V} or mock were cultured in 24-well plates in the absence of IL-3, whereas those transduced with Δ*Raf*-ER or mock were cultured under the same condition, except for the presence of 1 μM of 4-hydroxy-tamoxifen or a vehicle control (ethanol). The cells transduced with STAT5A1*6, STAT5#2 or none were purified on the basis of the expression of GFP using a FACS Aria (BD Biosciences) 36 h after infection. Immediately, these purified cells (1×10^4) were cultured in 96-well plates in the absence of IL-3, to avoid excessive signals caused by STAT5A#2 or 1*6 in the presence of IL-3, which led to cell death as described earlier.[25] Viable cell numbers were counted periodically after standard Trypan blue staining.

Leukemogenesis assays in vivo

Leukemogenesis assays *in vivo* using C57BL/6 mice produced by a combination of two kinds of transgenes were performed with lethal conditioning using lethally (9.5 Gy) irradiated recipients, or with sublethal conditioning using sublethally (5.25 Gy) irradiated recipients receiving no radioprotective bone marrow (BM) cells, as described earlier[6] (Supplementary Figure 1). In brief, hematopoietic progenitors were harvested from 6- to 10-week-old Ly-5.1 C57BL/6 mice 4 days after intraperitoneal administration of 150 mg/kg 5-fluorouracil, and cultured overnight in alpha minimal essential medium supplemented with 20% fetal calf serum and 50 ng/ml each of mouse stem cell factor, human IL-6, human FLT3-ligand (R&D Systems) and human thrombopoietin (Kirin Brewery, Takasaki, Japan). The prestimulated cells were infected with several combinations of the retroviruses for 60 h in the α minimal essential medium supplemented with the same fetal calf serum and cytokines using RetroNectin (Takara Bio Inc., Otsu, Japan) according to the manufacturer's recommendations, followed by intravenous injection of 10^5 of the cells into Ly-5.2 mice together with either a radioprotective dose (2×10^5) of Ly-5.2 cells under lethal conditioning or none under sublethal conditioning. Morbid mice and their tissue samples were analyzed, and immunophenotyping of BM, splenic and thymic cells was performed using the FACS Calibur, as described earlier.[33] The hematopoietic neoplasms were diagnosed mainly on the basis of morphology as described earlier.[6] The probabilities of murine overall survival were estimated using Kaplan–Meier method and compared using the log-rank test. All animal studies were performed in accordance with the guidelines of the Animal Care Committees of the Institute of Medical Science, the University of Tokyo and the Mie University.

Southern blot analysis

Genomic DNA was extracted from spleens, digested with *Nhe*I or *Bam*HI for detecting proviral integration and clonality, respectively, and analyzed with the Neo or puro probe (Supplementary Figure 1) as described earlier.[34]

Reverse transcriptase-polymerase chain reaction (PCR)

Total RNA was extracted from cell lines, spleen or BM, and reverse transcribed to complementary DNA as described earlier.[6] The conditions, reagents for reverse transcriptase-PCR and the primers specific for *β*$_2$*microglobulin* (*β*$_2$*MG*), *Hoxa9* and *MLL-SEPT6* have been described earlier,[6] except that PCR amplification for *MLL-SEPT6* transcripts was sometimes run for 35 cycles. To detect the transcript of *NRAS*^{G12V}, PCR amplification was run for 21 cycles using the following primers: *NRAS-S*, 5′-GTGGTTATAGATGGTGAAACCTGTT-3′ and *NRAS-AS*, 5′-GACCATAGGTACATCTTCAGAGTCCT-3′.

Results

MLL-SEPT6 *cooperates with both types of* FLT3 *mutations through different modes of signal transduction*

To clarify the molecular mechanism of cooperation between *MLL* fusion proteins and *FLT3* mutants, signaling pathways of *FLT3*-ITD and *FLT3*-TKD that cooperate with *MLL-SEPT6* were examined using the IL-3-dependent *MLL-SEPT6*-immortalized cell line, HF6.[6] Earlier, STAT5 and MAPK ERK1/2 had been found to be activated downstream of *FLT3* mutants in factor-dependent cell lines.[23,24] Therefore, the activation of these molecules was first examined using parental HF6 and transformed HF6 cells expressing FLT3-*ITD* (HF6^{ITD}) or *FLT3*^{D835V} (HF6^{D835V}) described earlier.[6] Nearly equal levels of expression of the *FLT3* mutants in the transformed HF6 cells were confirmed (Figure 1a). A western blot analysis after immunoprecipitation of the lysates from these cells revealed constitutive phosphorylation of STAT5A in HF6 cells expressing the FLT3 mutants in the absence of IL-3, but little in the parental HF6 cells that had been deprived of IL-3 (Figure 1b). In addition, a western blot analysis of the same lysates also revealed constitutive phosphorylation of ERK1/2 in those cells expressing the *FLT3* mutants, but little in the parental HF6 cells that had been deprived of IL-3 (Figure 1b).

Next, to determine whether STAT5 and/or MAPK were important in the transformation of HF6 cells expressing *FLT3* mutants, each signaling pathway was inhibited using dnSTAT5A or MEK inhibitor U0126. After retroviral transduction with the dnSTAT5A, the proliferation of HF6^{ITD} cells expressing dnSTAT5A was suppressed more efficiently than that of HF6^{D835V} cells expressing dnSTAT5A (Figure 2a). KO-positive cells expressing dnSTAT5A showed higher levels of phosphorylated STAT5 than KO-negative cells (Figure 2b). This finding is consistent with the earlier report showing that the dnSTAT5A exerts its effect on endogenous STAT5A and 5B with persistent phosphorylation of the dnSTAT5A itself.[35] In contrast, U0126 retarded the proliferation of the HF6^{D835V} cells more effectively than the HF6^{ITD} cells (Figure 2c, each IC50 is 0.67 ± 0.35 μM for HF6^{D835V} and 6.09 ± 0.90 μM for HF6^{ITD} in the absence of IL-3). Indeed, U0126 inhibited phosphorylation of ERK1/2 in the HF6^{ITD} and HF6^{D835V} cells in a semidose-dependent manner (Figure 2d). In addition, another important signaling pathway downstream of *FLT3*, through PI3 kinase, was inhibited using LY294002. LY294002 also retarded the growth of the HF6^{D835V} and HF6^{ITD} cells in a dose-dependent manner, but there was no remarkable difference between both types of HF6 cells (Supplementary Figure 2, each IC50 is 4.18 ± 0.55 μM for HF6^{D835V} and 8.12 ± 1.54 μM for HF6^{ITD} in the absence of IL-3).

Taken together, these results *in vitro* suggested that the activation of MAPK was more critical for transformation by *FLT3*-TKD than by *FLT3*-ITD in HF6 cells, whereas activation of STAT5 was more critical for transformation by *FLT3*-ITD than by *FLT3*-TKD.

Activation of Ras-MAPK cascade enables HF6 cells to grow without IL-3 through cooperation between Hoxa9 *and Raf*

We further examined whether direct activation of either STAT5 or MAPK cascade is sufficient to confer factor-independent